Extracellular Ca^{2+} Modulates the Effects of Protons on Gating and Conduction Properties of the T-type Ca^{2+} Channel α_{1G} ($Ca_V3.1$)

Karel Talavera,[1] Annelies Janssens,[1] Norbert Klugbauer,[2] Guy Droogmans,[1] and Bernd Nilius[1]

[1]Laboratorium voor Fysiologie, Campus Gasthuisberg, KU Leuven, B-3000 Leuven, Belgium
[2]Institut für Pharmakologie und Toxikologie, Technische Universität München, D-80802 München, Germany

ABSTRACT Since Ca^{2+} is a major competitor of protons for the modulation of high voltage–activated Ca^{2+} channels, we have studied the modulation by extracellular Ca^{2+} of the effects of proton on the T-type Ca^{2+} channel α_{1G} ($Ca_V3.1$) expressed in HEK293 cells. At 2 mM extracellular Ca^{2+} concentration, extracellular acidification in the pH range from 9.1 to 6.2 induced a positive shift of the activation curve and increased its slope factor. Both effects were significantly reduced if the concentration was increased to 20 mM or enhanced in the absence of Ca^{2+}. Extracellular protons shifted the voltage dependence of the time constant of activation and decreased its voltage sensitivity, which excludes a voltage-dependent open pore block by protons as the mechanism modifying the activation curve. Changes in the extracellular pH altered the voltage dependence of steady-state inactivation and deactivation kinetics in a Ca^{2+}-dependent manner, but these effects were not strictly correlated with those on activation. Model simulations suggest that protons interact with intermediate closed states in the activation pathway, decreasing the gating charge and shifting the equilibrium between these states to less negative potentials, with these effects being inhibited by extracellular Ca^{2+}. Extracellular acidification also induced an open pore block and a shift in selectivity toward monovalent cations, which were both modulated by extracellular Ca^{2+} and Na^+. Mutation of the EEDD pore locus altered the Ca^{2+}-dependent proton effects on channel selectivity and permeation. We conclude that Ca^{2+} modulates T-type channel function by competing with protons for binding to surface charges, by counteracting a proton-induced modification of channel activation and by competing with protons for binding to the selectivity filter of the channel.

KEY WORDS: pH • activation • permeation • selectivity • kinetic model

INTRODUCTION

At present, there are several lines of evidence that permeant ions modulate T-type Ca^{2+} channel gating. Shuba et al. (1991) showed that the mean open time of the T-type channel of mouse neuroblastoma cells depends on the type and concentration of the permeant ion and proposed that the channel region controlling channel closure senses a smaller fraction of the electric field due to a dynamic interaction between the ionic flux and the selectivity filter. In frog-atrial cardiomyocytes, Alvarez et al. (2000) showed that channel reopening after strong depolarizing prepulses was enhanced in low-Na^+ extracellular solutions and proposed that a competition between Na^+ and Ca^{2+} for binding sites within the channel modulates the amplitude of the voltage-facilitated T-type current. It is also known that the α_{1G} clone ($Ca_V3.1$) shows faster macroscopic inactivation in the presence of Ba^{2+} than in Ca^{2+} (Klugbauer et al., 1999; Staes et al., 2001).

T-type Ca^{2+} channels are also modulated by extracellular protons. Tytgat et al. (1990) reported that, in guinea pig cardiomyocytes, low extracellular pH (pH_e) induced a positive shift in the voltages for half-maximal activation (V_{act}) and inactivation (V_{inac}) together with an increase in the slope factor of channel activation (s_{act}). In a recent paper, Delisle and Satin (2000) concluded that proton block of T-type currents (α_{1H}, $Ca_V3.2$) under physiological conditions is due to gating modifications. These authors related the shift in the voltage for half-maximal activation by high extracellular proton concentrations to the titration of negative surface charges. To explain the increased slope factor of activation, they proposed that external acidification titrates some of the charges involved in the voltage sensing, but suggested already to test the influence of intrapore ions on the gating mechanisms.

Protons have also been shown to affect the open pore conduction of T-type channels. Tytgat et al. (1990) showed that extracellular acidification from pH 9.0 to 6 decreases the single channel conductance of the cardiac T-type channel of the guinea pig using 110 mM Ca^{2+} as charge carrier. For the α_{1H} T-type clone, Delisle and Satin (2000) found that open pore block was not the main determinant for the inhibition of whole-cell cur-

Karel Talavera's permanent address is Instituto de Cardiologia y Cirusia Cardiovascular, 10400 Lattabana, Cuba.

Address correspondence to Karel Talavera, Laboratorium voor Fysiologie, Campus Gasthuisberg, KU Leuven, B-3000 Leuven, Belgium. Fax: (32) 16 34 59 91; E-mail: karel.talavera@med.kuleuven.ac.be

rents by extracellular protons in the presence of 2.5 mM extracellular Ca^{2+} and 140 mM Na^+. They reported a negative shift of the reversal potential after extracellular acidification and suggested that channel protonation shifts channel selectivity toward monovalent ions.

Protons have been shown to modulate the gating processes of high voltage–activated (HVA)* Ca^{2+} channels (Pietrobon et al., 1989; Prod'hom et al., 1989; Kwan and Kass, 1993; Tombaugh and Somjen, 1996; Zhou and Jones, 1996; Smirnov et al., 2000; Shah et al., 2001). In these channels, Ca^{2+} has been shown to be a major competitor of protons for the neutralization of surface charges (Kwan and Kass, 1993) and for binding to pore residues that control ion permeation and selectivity (Chen et al., 1996; Chen and Tsien, 1997). To achieve further insight in the mechanisms of ionic modulation of T-type channel function, we investigated the influence of the extracellular Ca^{2+} concentration ($[Ca^{2+}]_e$) on the proton-induced modifications of gating and permeation mechanisms of the α_{1G} T-type subunit and the role of the selectivity filter (the EEDD pore locus) in the modulation of channel selectivity and permeation by protons. Our results suggest for three substrates of competition between Ca^{2+} and protons, resulting in modifications of channel gating and ionic conduction.

MATERIALS AND METHODS

Solutions

Before current recordings, cells were rinsed with Krebs solution containing: 150 mM NaCl, 6 mM KCl, 1 mM $MgCl_2$, 1.5 mM $CaCl_2$, 10 mM glucose, 10 mM HEPES, and titrated to pH 7.4 with 1 N NaOH. All extracellular test solutions contained 5 mM CsCl, 5 mM glucose, a mixture of MES, HEPES, and TAPS (5 mM each) to extend the buffering range from pH 5.5 to 9.1, and were kept Mg^{2+} free to avoid extracellular Mg^{2+} block (Serrano et al., 2000). We used extracellular solutions of 2 or 20 mM $CaCl_2$ or a Ca^{2+} free solution (5 mM EDTA) with 20 mM NaCl, osmotically compensated with 150, 120, or 130 mM NMDG, respectively. To assess the influence of Na^+ on conduction properties in the 2 mM Ca^{2+} solution, 150 mM NMDG was substituted by an equimolar amount of Na^+. Test solutions containing NMDG were titrated with HCl and those containing 150 mM NaCl with CsOH. When 2 or 20 mM Ca^{2+} solutions were used, the intracellular (pipette) solution contained 102 mM CsCl, 10 mM HEPES, 5 mM $MgCl_2$, 5 mM Na_2-ATP, 10 mM TEA-Cl, 10 mM EGTA, titrated to pH 7.4 with 1 N CsOH. In the experiments in zero $[Ca^{2+}]_e$ the intracellular solution did not contain $MgCl_2$ and Na_2-ATP in order to avoid block by Mg^{2+} and to limit the size of outward currents, respectively. All chemicals were purchased from Sigma-Aldrich.

Electrophysiology

We used human embryonic kidney cells (HEK293) grown and transfected with the wild-type α_{1G} (Klugbauer et al., 1999) or the EEED pore mutant as in previous works (Staes et al., 2001; Talavera et al., 2001). Currents were recorded in the whole-cell configuration of the patch-clamp technique using an EPC-7 (LIST Electronics) patch-clamp amplifier and filtered with an eight-pole Bessel-filter (Kemo). For control of voltage-clamp protocols and data acquisition, we used an IBM-compatible PC with a TL-1 DMA interface (Axon Instruments, Inc.) and the software pCLAMP (Axon Instruments, Inc.). Bath solutions were perfused by gravity via a multibarreled pipette. Patch pipettes were pulled from Vitrex capillary tubes (Modulohm) using a DMZ-Universal puller (Zeitz-instruments). An Ag-AgCl wire was used as reference electrode. Adequate voltage control was achieved by using low pipette resistances (1–2.5 MΩ) and series resistance compensation to the maximum extent possible (50–70%). Membrane-capacitive transients were electronically compensated and the linear background components were digitally subtracted before data analysis. Current traces were filtered at 2.5–5 kHz and digitized at 5–10 kHz. All experiments were performed at room temperature (22–25°C).

Stimulation Protocols and Data Analysis

I-V curves were obtained from the peak amplitude of currents evoked by the application 200-ms lasting voltage steps from −90 to 60 mV. These curves were fitted with:

$$I(V) = G(V)\cdot(V - V_r)\left\{\frac{A}{1+\exp[-(V - V_{act})/s_{act}]} + \frac{1-A}{1+\exp[-(V - V'_{act})/s'_{act}]}\right\}, \quad (1)$$

where I is the measured peak current, V the step potential and $G(V)$ the conductance, which may be voltage dependent. The activation curves in 2 and 20 mM Ca^{2+} solutions were best described by the sum of two Boltzmann components (Serrano et al., 1999; Lacinova et al., 2002). V_{act} and V'_{act} are the potentials of half-maximal amplitude, s_{act} and s'_{act} are the slope parameters and A is the amplitude of the steeper component. In Ca^{2+} free solutions only one Boltzmann function was needed ($A = 1$). To account for the strong inward rectification in the 2 and 20 mM Ca^{2+} solutions, we have approximated G(V) from a fit of the amplitudes of the tail current after a depolarizing step to 100 mV in the voltage range from −70 to 110 mV for α_{1G} and from −70 to 70 mV for the EEED mutant with the equation:

$$I_{tail}(V) = G(V)\cdot(V - V_r), \quad (2)$$

with $G(V) = G\cdot(V^2 + b\cdot V + c)$. The I-V relation in the Ca^{2+} free, 20 mM Na^+ extracellular solution is fairly linear, and hence $G(V) = G$.

The average values of the fit parameters b and c for each experimental condition were then used to fit the I-V curves with Eq. 1. We noticed that an adequate description of the open pore conduction was essential for an accurate estimation of the slope factor s_{act} of the activation curve, and that the use of the classical linear function for $G\cdot(V - V_r)$ in Eq. 1 consistently overestimated the values for s_{act} for the currents in 2 or 20 mM Ca^{2+}. Activation curves were calculated by dividing the experimental I-V curves by the appropriate $G(V)\cdot(V - V_r)$ function in each experimental condition.

The time constants of activation (τ_{act}) and inactivation (τ_{inac}) were determined from a fit of current traces with the equation:

$$I(t) = I_m\cdot[1 - \exp(-t/\tau_{act})]^2\cdot\exp(-t/\tau_{inac}) + I_b, \quad (3)$$

Abbreviation used in this paper: HVA, high voltage–activated.

where I_m is a normalization factor and I_b is a background component. Given the sampling rate used in the activation protocol, the values of τ_{act} at positive voltages (<0.5 ms) should be considered as an upper limit of the real values. Nevertheless, our estimates are equal or smaller than previously reported values (0.6 ms, Nilius, 1992; 0.3 ms, Chen and Hess, 1990). The decaying phase of the voltage dependence of τ_{act} was fitted with an exponential function of the form:

$$\tau_{act}(V) = \exp[-(V - V\tau_{act})/(s\tau_{act})] + \tau_{act}(\infty), \quad (4)$$

where $s\tau_{act}$ is the voltage sensitivity, $\tau_{act}(\infty)$ is the asymptotic value at positive potentials and $V\tau_{act}$ is the voltage at which τ_{act} is equal to $1 + \tau_{act}(\infty)$.

Steady-state inactivation (h_∞) was determined from the peak current recorded during a 160-ms test pulse to 0 mV after a 5,120-ms lasting prepulses to potentials between −100 and −25 mV. The voltage dependence of these peak currents, normalized to that following the prepulse to −100 mV, was fitted with the equation:

$$h_\infty(V) = \frac{1}{1 + \exp[(V - V_{inac})/s_{inac}]}, \quad (5)$$

where V_{inac} is the potential of half-maximal inactivation and s_{inac} the slope factor for the inactivation.

To dissect the effects of ionic conditions on conduction properties from those on gating, tail currents were recorded during voltage steps between −120 and 110 mV after a 7.5-ms lasting depolarization to 100 mV to normalize for the positive voltage shift of the steady-state activation at low pH_e. Linear background components and capacitive transients were subtracted by the application of a −P/4 protocol. In the presence of 2 mM Ca^{2+} there was an ~10% decrease in the estimated maximal open probability during the prepulse to 100 mV when the pH_e was changed from 9.1 to 6.2. However, at 7.5 ms the estimated open probability was not significantly different between these conditions (unpublished data). This ensured that the changes in the amplitude of the tail currents with the extracellular perfusion condition were determined by open pore properties and not by modifications in gating during the prepulse to 100 mV. We determined the amplitude (I_{tail}) and time constant of current decay (τ_{decay}) from a single-exponential fit of the time course of the tail currents. τ_{decay} corresponds to the time constant of deactivation (τ_{deac}) at negative potentials and to the time constant of the macroscopic inactivation (τ_{inac}) at potentials positive to the activation threshold. The usual way to characterize the voltage dependence of τ_{deac} is to fit τ_{decay}(V) with a growing exponential function in a range of very negative potentials. This approximation is expected to underestimate the steepness of the voltage dependency of τ_{deac} since it does not consider the contribution of the inactivation to current decay. Additional underestimation of the steepness may occur when fitting tail currents at very negative potentials given that the estimated values of τ_{decay} tend to be higher than the actual ones due to voltage clamp errors that are the consequence of large tail current amplitudes. When considering the current models of T-type channel gating (see Fig. 13), in a second order of approximation, the voltage dependence of τ_{decay} can be expressed by:

$$\tau_{decay}(V) = \frac{1}{\exp[-(V - V\tau_{deac})/(s\tau_{deac})] + k_{OIo}}, \quad (6)$$

where V is the repolarization potential, $V\tau_{deac}$ the voltage at which τ_{deac} is equal to 1 ms, $s\tau_{deac}$ the voltage sensitivity of the time con-

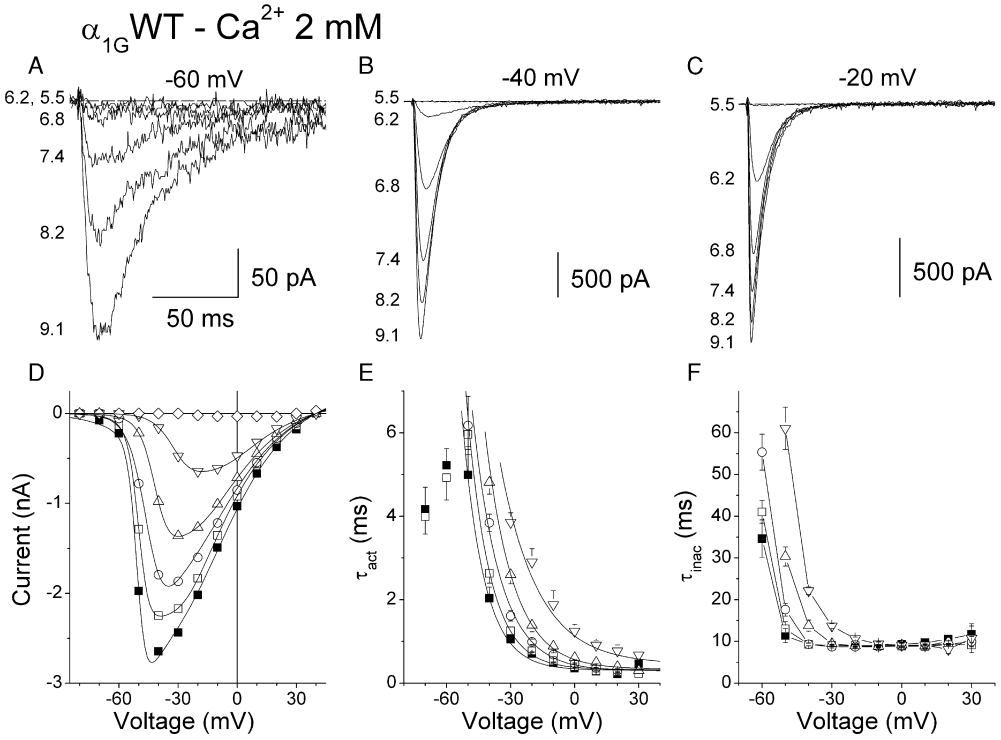

FIGURE 1. Proton inhibition of α_{1G} currents in the presence of 2 mM extracellular Ca^{2+}. (A–C) Typical proton effects on current traces evoked by voltage steps to −60, −40, and −20 mV, respectively. The labels at the left of each trace indicate the pH_e at which they were registered. (D) Voltage dependence of the amplitude of the traces shown in the top panels. Continuous lines are the best fit of the data with Eq. 1. (E) pH_e modulation of the voltage dependence of the time constant of activation (τ_{act}) (n = 5–6). The decaying phase of τ_{act}(V) was fitted with Eq. 4. Data points of the raising phase of τ_{act}(V) at pH_e 7.4, 6.8, and 6.2 are not shown for clarity. (F) pH_e effects on the voltage dependence of the time constant of macroscopic inactivation (τ_{inac}). In D–F symbols apply to pH_e values as follows: 9.1, ■; 8.2, □; 7.4, ○; 6.8, △; 6.2, ▽; 5.5, ◇.

stant of deactivation, and k_{OIo} is the rate constant of the transition between the open state (O) and the closest inactivated state (I_O). This approximation is proved to be valid as the channels have low probability of being in the closed state (C_3) near the open state and the inactivation process is largely absorbing ($k_{OIo} >> k_{IoO}$) (see Fig. 13).

In all voltage protocols the holding potential was −100 mV and the stimulation frequency 0.5 Hz, with the exception of the inactivation protocol in which it was 0.2 Hz. Electrophysiological data were analyzed using the WinASCD software package (ftp://ftp.cc.kuleuven.ac.be/pub/droogmans/winascd.zip; G. Droogmans, Laboratory of Physiology, KU Leuven). For all measurements pooled data are given as mean ± SEM. We used ANOVA and Student's paired *t* test, taking $P < 0.05$ or $P < 0.01$ as the level of significance.

Data Simulation

We used MATLAB (MathWorks) to solve a Markov model for the gating of α_{1G} in several pH_e, in the presence of 2 or 20 mM Ca^{2+}. Parameter optimization and numerical solution of the differential equations were performed with the built-in functions *fmin* and *expm*, respectively.

RESULTS

Effects of pH_e and Extracellular Ca^{2+} on the Activation of α_{1G}

We tested the modulation of the gating of α_{1G} by extracellular Ca^{2+} and protons by studying the effects of pH_e in the range from 9.1 to 5.5 on I-V curves in the presence of 0, 2, or 20 mM Ca^{2+}. Fig. 1, A–C, shows current traces at various pH_e values in the presence of 2 mM Ca^{2+} during voltage steps to −60, −40, and −20 mV. Current reduction at low pH_e was most pronounced at more negative potentials. As a consequence, the I-V curve, derived from the peak current amplitudes, was shifted in the positive direction at lower pH_e (Fig. 1 D). Fig. 1, E and F, shows that extracellular acidification also shifts the voltage dependence of the time constants of activation (τ_{act}) and macroscopic inactivation (τ_{inac}).

These effects of pH_e were less prominent in 20 mM Ca^{2+} (Fig. 2, A–C). Acidification significantly inhibited the inward current, but the block was still incomplete at pH_e 5.5. The shift of the peak I-V curve and of the voltage dependence of τ_{act} and τ_{inac} were also much smaller than in 2 mM Ca^{2+} (Fig. 2, D–F).

The effects of pH_e were most pronounced in the absence of extracellular Ca^{2+} (5 mM EDTA). Under these conditions, T-type Ca^{2+} channels, like HVA Ca^{2+} channels, conduct large currents of monovalent cations (Carbone and Lux, 1987; Talavera et al., 1998; Alvarez et al., 2000). Fig. 3, A–C, shows current traces recorded at pH_e values ranging from 9.1 to 5.5 during voltage pulses to −80, −60, and 0 mV, respectively. The current at −80 mV was completely inhibited by changing pH_e from 9.1 to 8.2, but further acidification was necessary to fully block the current at less negative potentials. Because of the reduced extracellular Na^+ concentration (20 mM), currents were outward at potentials positive to −15 mV. The current at 0 mV was completely inhibited only at pH_e 5.5. The voltage shift of the I-V curves due to external acidification was more pronounced than in the presence of 2 or 20 mM Ca^{2+} (Fig. 3 D). Remarkably, a reduction of pH_e from 9.1 to 7.4 induced a positive shift of the voltage of the peak inward current

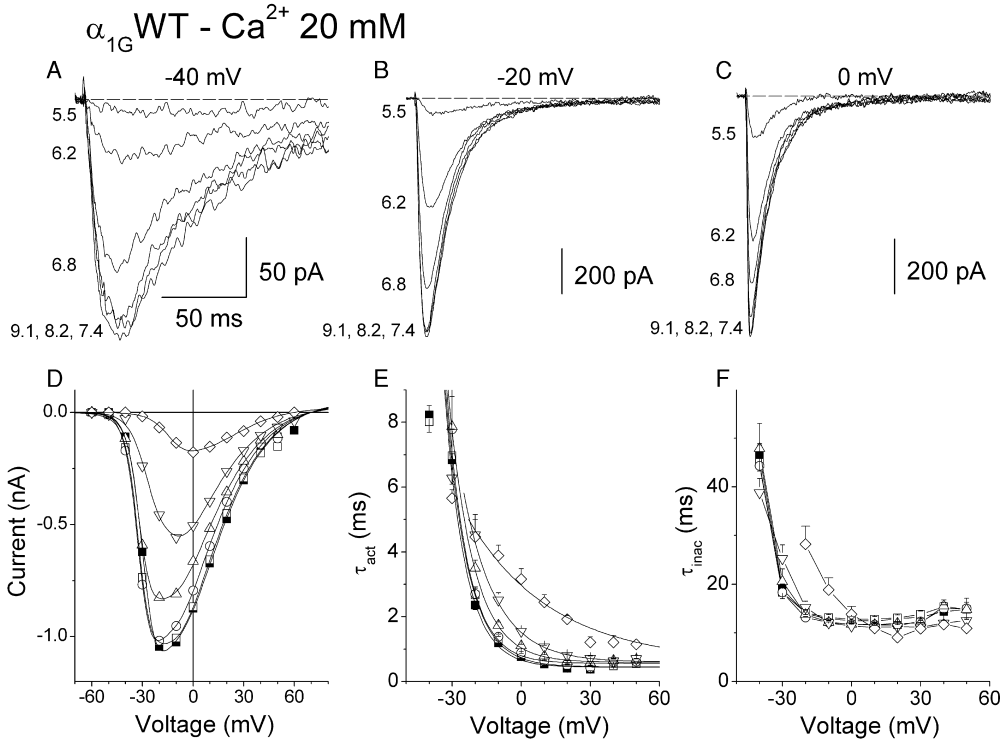

FIGURE 2. Proton inhibition of α_{1G} currents in 20 mM extracellular Ca^{2+}. (A–C) Typical proton effects on current traces evoked by voltage steps to −40, −20, and 0 mV, respectively. The pH_e is indicated at the left of each trace. (D) I-V curves corresponding to the traces shown in the top panels. Continuous lines are the best fits of the data with Eq. 1. (E and F) pH_e effects on the voltage dependencies of the time constants of activation (τ_{act}) and inactivation (τ_{inac}) (n = 5–7). Data points of the raising phase of τ_{act}(V) at pH_e values from 7.4 to 5.5 are not shown for clarity. The decaying phase of τ_{act}(V) was fitted with Eq. 4. In D–F symbols apply to pH_e values as follows: 9.1, ■; 8.2, □; 7.4, ○; 6.8, △; 6.2, ▽; 5.5, ◇.

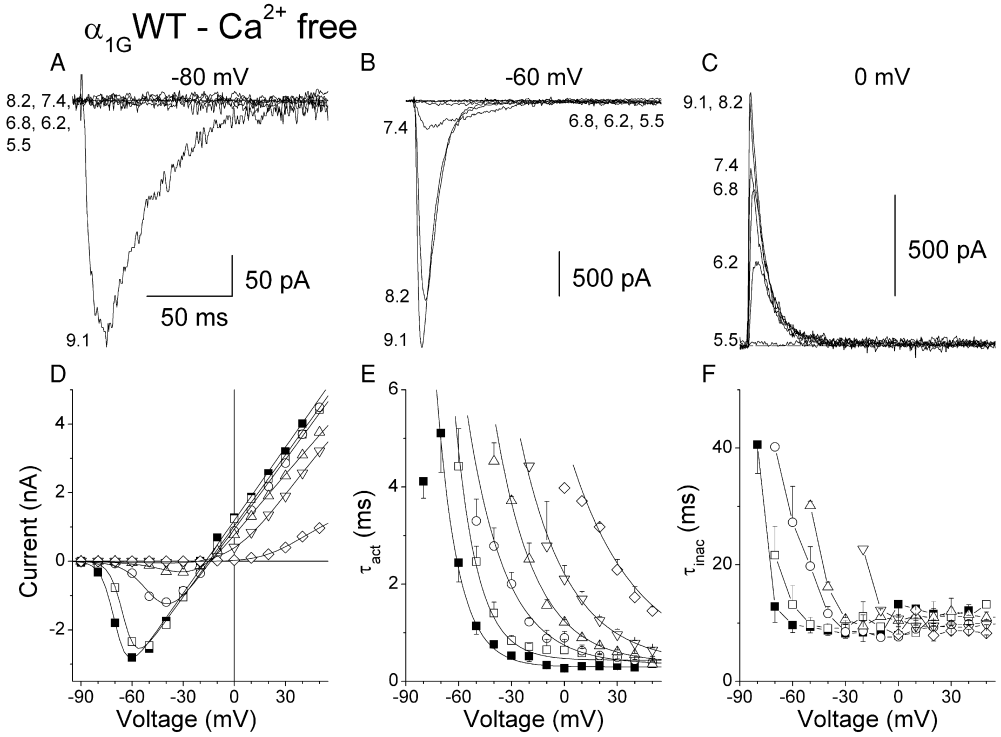

FIGURE 3. Proton inhibition of α_{1G} currents in zero Ca^{2+}. (A–C) Typical proton effects on current traces evoked by voltage steps to −80, −60, and 0 mV, respectively. Numbers at the left of each trace indicate the pH_e at which they were registered. (D) *I-V* curves corresponding to the traces shown in the top panels. Continuous lines are the best fits with Eq. 1. (E) pH_e modulation of the voltage dependence of the time constant of activation (τ_{act}) (n = 3–5). The decaying phase of τ_{act}(V) was fitted with Eq. 4. Data points of the raising phase of τ_{act}(V) at pH_e values from 8.2 to 5.5 are not shown for clarity. (F) pH_e effects on the voltage dependence of the time constant of macroscopic inactivation (τ_{inac}). In D–F pH_e values are symbolized as follows: 9.1, ■; 8.2, □; 7.4, ○; 6.8, △; 6.2, ▽; 5.5, ◇.

by ~20 mV, and inward currents were almost completely inhibited at pH_e 6.2. The effects of protons on the voltage dependences of τ_{act} and τ_{inac} were clearly more pronounced than in the presence of 2 or 20 mM Ca^{2+} (Figs. 3, E and F, see below).

Fig. 4 A shows the effects of protons on the voltage-dependence of α_{1G} activation in the presence of 0, 2, and 20 mM Ca^{2+}. The extracellular acidification to pH 6.2 did not only shift the activation curve to depolarized potentials, but also reduced its slope. It is remarkable that this effect of acidification on the slope of the activation curve, which is incompatible with a screening of surface charges by protons, was much larger in the absence of extracellular Ca^{2+}.

Activation curves were best described by two Boltzmann components in 2 and 20 mM Ca^{2+}. The amplitude (1–A) and the slope factor (s'_{act}) of the shallower component were around 0.45 and 8 mV, respectively, and were pH_e and $[Ca^{2+}]_e$ independent (unpublished data). The voltage for half-maximal activation of both components (V_{act} and V'_{act}) showed identical pH_e and $[Ca^{2+}]_e$ dependencies. Therefore, we only show in detail the results regarding the modification of the steeper Boltzmann component. V_{act} depends on both pH_e and $[Ca^{2+}]_e$, as shown in Fig. 4 B. Changing pH_e from 9.1 to 6.2 shifted V_{act} by ~80 mV in the absence of Ca^{2+}, and by ~20 and 10 mV in the presence of 2 or 20 mM Ca^{2+}, respectively. The values of V_{act} in 2 and 20 mM Ca^{2+} seem to converge at low pH_e, suggesting that protons and Ca^{2+} may compete for the same binding sites. A peculiar finding is that the curves representing V_{act} as a function of pH_e in Ca^{2+}-free solution and those in 2 or 20 mM Ca^{2+} intersect, the values for V_{act} in Ca^{2+}-free solutions being more negative at alkaline pH_e (>6.8) and more positive at acidic pH_e (see also Fig. 4 A). This observation is incompatible with the neutralization of surface charges by competing Ca^{2+} and protons as the only mechanism underlying the voltage shift of channel activation.

The slope factor of the steeper component of the activation s_{act} increased with extracellular acidification, an effect that is antagonized by increasing $[Ca^{2+}]_e$ (Fig. 4 C). Reducing pH_e from 9.1 to 7.4 significantly increased s_{act} in 2 mM Ca^{2+}, whereas acidification to pH_e 6.2 and below was necessary to affect s_{act} in 20 mM Ca^{2+}. Also the values of s_{act} in 2 and 20 mM Ca^{2+} seem to converge at low pH_e. The changes in s_{act} were much more dramatic in the absence of Ca^{2+}, since this parameter increased about fourfold if pH_e was changed from 9.1 to 6.2.

The rightward shift and increased slope factor of the activation curve by extracellular acidification might result from a voltage-dependent open pore block (Woodhull, 1973). Such a mechanism would, however, not affect the kinetics of channel activation, and is in contrast with the observed shift of the voltage dependences of the time constants of activation τ_{act} and macroscopic inactivation τ_{inac} (Figs. 1–3). The rightward

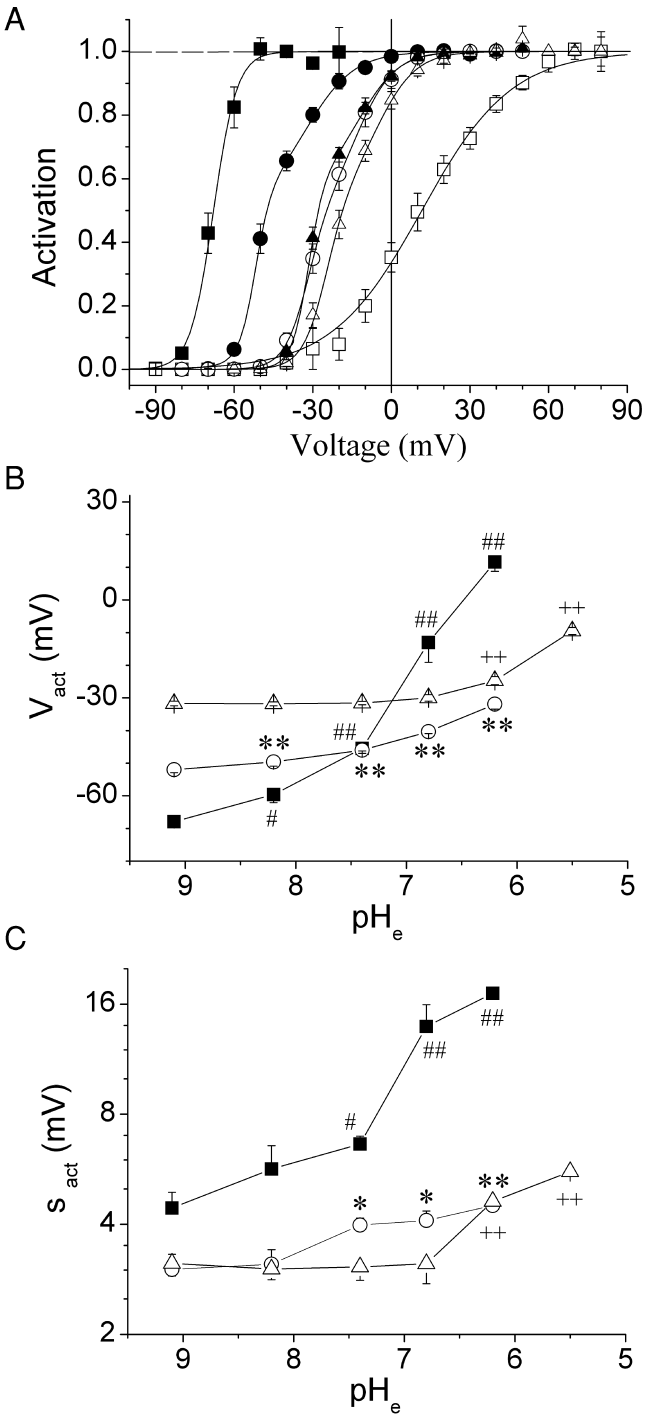

FIGURE 4. Summary of proton effects on the activation curve of α_{1G} in 0, 2, and 20 mM extracellular Ca^{2+}. (A) Average activation curves obtained at pH_e 9.1 (filled symbols) and 6.2 (open symbols), in 0 (■, □), 2 (●, ○), or 20 (▲, △) mM Ca^{2+}. Continuous lines are the activation curves calculated from the average values of the parameters obtained from the fit of I-V curves with Eq. 1 in each experimental condition. (B and C) Effects of pH_e on V_{act} and s_{act}. Labels (#), (*), and (+) indicate significant difference with $P < 0.05$ from the values of V_{act} and s_{act} obtained at pH_e 9.1 for 0 (■), 2 (○), and 20 (△) mM Ca^{2+} conditions, respectively. Double labels indicate significant difference with $P < 0.01$.

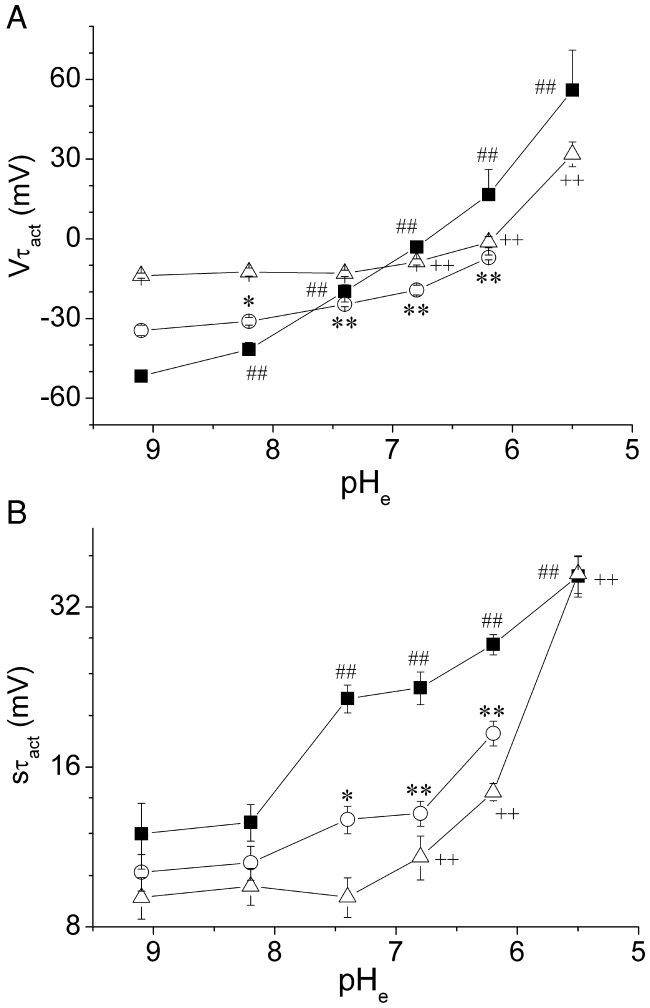

FIGURE 5. Proton effects on the time constant of activation of α_{1G} are Ca^{2+} dependent. (A and B) pH_e dependencies of $V\tau_{act}$ and $s\tau_{act}$, respectively. Labels (#), (*), and (+) indicate significant difference with $P < 0.05$ from the values obtained at pH_e 9.1 for 0 (■), 2 (○), and 20 (△) mM Ca^{2+} conditions, respectively. Double labels indicate significant difference with $P < 0.01$.

shift of the voltage dependence of τ_{act} at pH_e 9.1 by increasing $[Ca^{2+}]_e$ is consistent with a mechanism of screening of surface charges by Ca^{2+}. However, the observation that a decrease of pH_e did not only shift the voltage dependence of τ_{act} to more positive voltages but also decreased its slope is inconsistent with simple screening by protons. To quantify these effects, we have estimated the position of the curve $\tau_{act}(V)$ along the voltage axis ($V\tau_{act}$), and the steepness of the voltage dependence ($s\tau_{act}$) from the fit of the data points of the decaying phase with Eq. 4 for each experimental condition. Fig. 5, A and B, show that the patterns of modulation of the pH_e dependence of $V\tau_{act}$ and $s\tau_{act}$ by extracellular Ca^{2+} are similar to those of V_{act} and s_{act} (compare with Fig. 4, B and C). This indicates that the Ca^{2+}-dependent inhibition of α_{1G} by protons is to a large

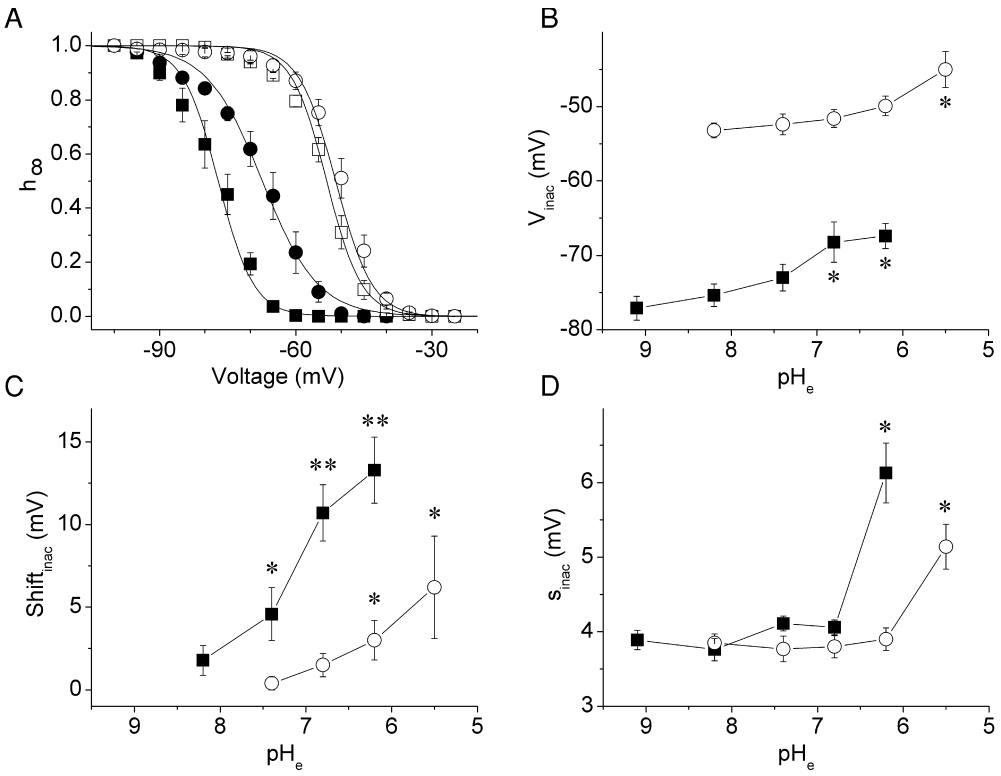

FIGURE 6. $[Ca^{2+}]_e$ and pH_e dependency of steady-state inactivation of α_{1G}. (A) Average inactivation curves obtained in 2 mM (filled symbols, n = 4–10) or in 20 mM Ca^{2+} (open symbols, N = 5–9) at different pH_e (9.1, ■; 8.2, □; and 6.2, ●,○). Continuous lines are the inactivation curves calculated from Eq. 5 using the average values of V_{inac} and s_{inac} determined for each experimental condition. (B) pH_e dependence of the average V_{inac} in the presence of 2 (■) or 20 (○) mM Ca^{2+}. (C) average shift of inactivation curves respect to the curves obtained at pH_e 9.1 and 8.2, in 2 (■) or 20 (○) mM Ca^{2+}, respectively. (D) average slope factor of the steady-state inactivation as function of pH_e in 2 (■) or 20 (○) mM Ca^{2+}. In B and D the label (*) indicates significant difference with $P < 0.05$ from the values obtained at pH_e 9.1 (Ca^{2+} 2 mM) or pH_e 8.2 (Ca^{2+} 20 mM). In C the labels (*) and (**) denote significant difference from zero with $P < 0.05$ and $P < 0.01$, respectively.

extent due to an effect of protons on gating. The issue of open pore block by protons and its Ca^{2+} dependence is addressed below.

Extracellular Ca^{2+} Modulates the Effect of Protons on Steady-state Inactivation of α_{1G}

Tytgat et al. (1990) reported that extracellular alkalinization induced a negative shift of the voltage dependence of steady-state inactivation of native T-type Ca^{2+} channels, and Delisle and Satin (2000) showed a positive shift with extracellular acidification in the human-cloned α_{1H} T-type channel. In this paper, we compared the effects of pH_e on the steady-state inactivation properties of α_{1G} in the presence of 2 or 20 mM Ca^{2+}. Because a change of pH_e from 9.1 to 8.2 in the presence of 20 mM Ca^{2+} did not affect channel activation, we used the results at pH_e 8.2 as a reference for the proton-induced changes in channel availability for this $[Ca^{2+}]_e$. For 2 mM Ca^{2+} the results at pH_e 9.1 were taken as reference. Fig. 6 A compares the changes in average channel availability after extracellular acidification from 9.1 to 6.2 in the presence of 2 mM Ca^{2+} and from 8.2 to 6.2 in 20 mM Ca^{2+}. The pH_e dependence of the average potential for half-maximal inactivation (V_{inac}), as estimated from the fits of the data points with Eq. 5, is shown in Fig. 6 B. To better characterize the changes in V_{inac}, we have averaged the voltage shifts of the individual cells. These results, plotted in Fig. 6 C, show that a change of pH_e from 9.1 to 7.4 or lower significantly shifts the availability curves at 2 mM Ca^{2+} to more positive potentials, but an acidification up to pH_e 6.2 was necessary to induce a significant shift at 20 mM Ca^{2+}. External acidification up to pH 6.8 in 2 mM Ca^{2+} did not significantly affect the slope factor of the inactivation process (s_{inac}, Fig. 6 D), but this factor was significantly increased at pH_e 6.2. In contrast, a significant effect on s_{inac} in 20 mM Ca^{2+} was only observed at pH_e 5.5.

pH_e-induced Changes on Activation and Inactivation Are Partially Correlated

The effects of pH_e on both processes of activation and inactivation of α_{1G} are consistent with the previously reported coupling between activation and macroscopic inactivation of single T-type Ca^{2+} channels (Droogmans and Nilius, 1989). We have therefore studied the correlation between the parameters describing the steady-state activation and inactivation when varying pH_e. Fig. 7 A shows the correlation between V_{inac} and V_{act} obtained at different pH_e values and at 2 or 20 mM Ca^{2+}. Assum-

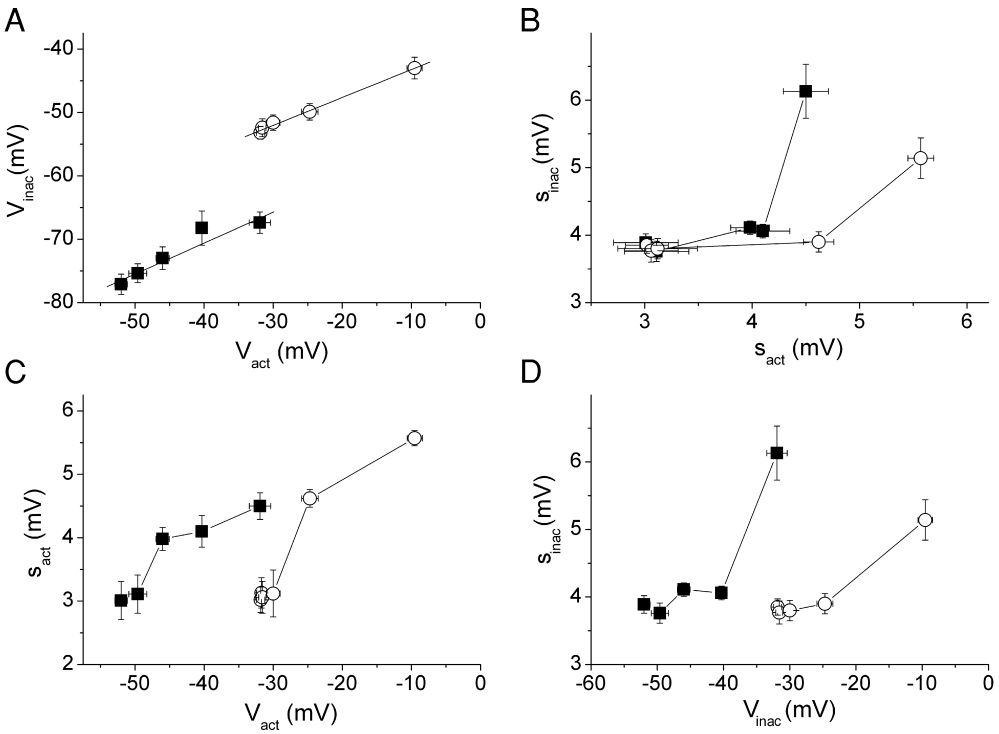

FIGURE 7. Proton-induced changes in activation and inactivation are not strictly coupled. Relation between the gating parameters describing steady-state activation and inactivation when pH_e is changed from 9.1 to 6.2 in 2 mM Ca^{2+} (■) and from 8.2 to 5.5 in 20 mM Ca^{2+} (○). (A) Correlation between the voltage for half-maximal inactivation V_{inac} and the voltage for half-maximal activation V_{act}. Continuous lines are the best fits obtained using the function $V_{inac} = m \cdot V_{act} + n$. In 2 mM Ca^{2+} m and n were equal to 0.45 ± 0.09 and −54 ± 4 mV, respectively, while in 20 mM Ca^{2+} were 0.40 ± 0.07 and −41 ± 2 mV, respectively. (B) Changes in s_{act} are not strictly correlated to changes in s_{inac}. (C) The changes in V_{act} are accompanied by changes in s_{act}. (D) Lack of strict correlation between the changes in V_{inac} and the voltage sensitivity of the steady-state inactivation (s_{inac}).

ing a linear relationship between V_{inac} and V_{act}, we obtained slopes of 0.49 ± 0.09 ($R = 0.97$) and 0.44 ± 0.08 ($R = 0.99$) at 2 and 20 mM Ca^{2+}, respectively. Proton-induced changes in s_{act} from 3.0 to 4.1 mV (in 2 mM Ca^{2+}) and from 3.0 to 4.6 mV (in 20 mM Ca^{2+}) were not paralleled by significant changes in s_{inac}, indicating that the voltage sensitivity of steady-state inactivation was less pH sensitive than that of activation (Fig. 7 B). On the other hand, proton-induced changes in V_{act} were consistently accompanied by changes in s_{act} (in both 2 and 20 mM Ca^{2+}), whereas changes in V_{inac} up to 12.7 mV (in 2 mM Ca^{2+}) or 8.5 mV (in 20 mM Ca^{2+}) did not correspond to significant changes in s_{inac} (Fig. 7, C and D).

The Effects of Extracellular Protons on Ion Permeation and Selectivity Depend on Extracellular Ca^{2+} and Na^+. Comparison between $\alpha 1G$ and the EEED Pore Mutant

Besides their effects on gating, extracellular protons alter ion permeation through T-type Ca^{2+} channels (Tytgat et al., 1990; Delisle and Satin, 2000). It has been shown that permeation and selectivity of Ca^{2+} channels depend on Ca^{2+} and Na^+ (Polo-Parada and Korn, 1997) and that T-type channels are less Ca^{2+} selective than HVA Ca^{2+} channels (Lee et al., 1999; Serrano et al., 2000). We were therefore interested to find out whether the effects of protons on ion permeation through α_{1G} were Ca^{2+} and/or Na^+ dependent.

We analyzed the effects of pH_e on the amplitude of α_{1G} tail currents in 2 mM Ca^{2+} (150 mM Na^+ or $NMDG^+$) or 20 mM Ca^{2+} (120 mM $NMDG^+$) (Fig. 8, A–C). Decreasing pH_e from 9.1 to 6.2 in 2 mM Ca^{2+} and 150 mM $NMDG^+$ significantly reduced inward tail currents, but did not affect outward currents (Fig. 8 A). The effects of pH_e on the inward currents were smaller if $NMDG^+$ was replaced by Na^+ (Fig. 8 B) or if $[Ca^{2+}]_e$ was increased to 20 mM (Fig. 8 C). To quantify the voltage dependence of this proton block, we have calculated at each potential and for each cell and Ca^{2+}-Na^+ condition the ratio of the current amplitudes at pH_e 6.2 and 9.1 (*I(pH6.2)/I(pH9.1)*, Fig. 8 D). Extracellular protons exerted a significant (≈33%) block of the current in 2 mM Ca^{2+} in the absence of extracellular Na^+. This block was voltage independent in the range from −120 to 20 mV and declined sharply around the reversal potential. The voltage range in which the block was voltage dependent was larger in 2 mM Ca^{2+} and 150 mM Na^+, but the maximal block was the same as in the Na^+ free solution. The proton block was significantly smaller at 20 mM Ca^{2+} (≈10%), indicating that extracellular Ca^{2+} antagonizes the effects of protons on ion conduction through α_{1G}.

We performed similar experiments using a pore mutant in which aspartate D1487 of the P-loop in domain III was substituted by glutamate, because the divalent

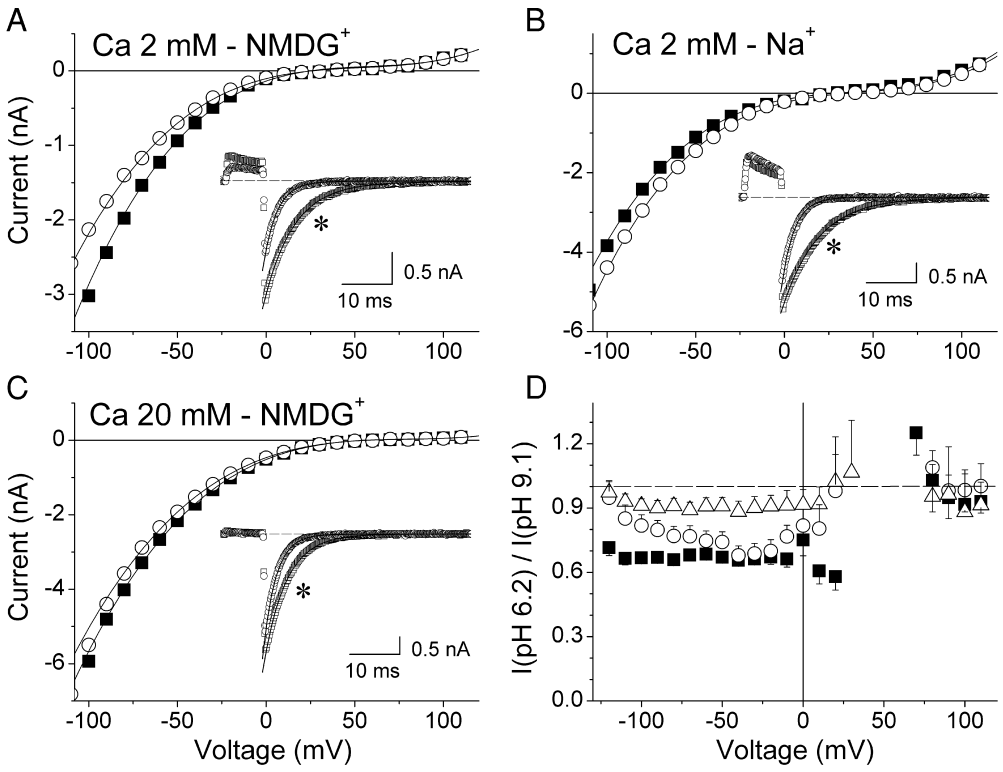

FIGURE 8. Open pore block by protons in α_{1G} is dependent on extracellular Ca^{2+} and Na^+ concentrations. Voltage dependence of the amplitude of tail currents through the wild-type channel α_{1G} at pH_e 9.1 (■) and 6.2 (○) in the presence of: A, 2 mM Ca^{2+} (150 $NMDG^+$); B, 2 mM Ca^{2+} (150 Na^+); and C, 20 mM Ca^{2+} (120 $NMDG^+$). Continuous lines are the best fits with Eq. 2 in the voltage range from −70 to 110 mV. Insets in A–C show current traces at −80 mV in the corresponding perfusion conditions. The asterisks denote the traces obtained at pH_e 9.1. The difference in current amplitude during the prepulse to 100 mV at pH_e 6.2 with respect to that at pH_e 9.1 (insets A and B) is mainly (∼90%) due to a background current. (D) Voltage dependence of the ratio between the amplitude of the tail currents recoded at pH_e 6.2 respect to those determined at pH_e 9.1 in the presence of 2 mM Ca^{2+} (150 $NMDG^+$) (■), 2 mM Ca^{2+} (150 Na^+) (○) or 20 mM Ca^{2+} (120 $NMDG^+$) (△) (n = 6–7).

over monovalent cation selectivity of this mutant channel (called EEED) is reduced, and because it is more sensitive to protons than the wild-type α_{1G} (Talavera et al., 2001). The maximum proton block of the mutant EEED in 2 mM Ca^{2+} and in the absence of Na^+ was similar to that of the wild-type (≈35%), but it was voltage-dependent over a much broader voltage range (Fig. 9, A and D). However, extracellular acidification significantly increased the amplitude of the tail currents in the presence of Na^+, indicating that channel protonation strongly enhances Na^+ conduction through the mutant channel (Fig. 9, B and D). Like for the wild type channel, proton block was smaller in 20 mM Ca^{2+} (≈20%, which was larger than in α_{1G}) and voltage dependent in the range from −100 to 0 mV (Fig. 9, C and D).

We can assess the effects of extracellular acidification on channel selectivity and its possible dependence on $[Ca^{2+}]_e$ from the reversal potentials (V_r) in the various experimental conditions. Fig. 10, A and B, show the average amplitudes of tail currents from cells expressing α_{1G} and the EEED mutant, respectively, at an expanded voltage scale in the region of V_r. Extracellular acidification shifted the V_r of α_{1G} to less positive values in 2 mM Ca^{2+} but not in 20 mM Ca^{2+} (Fig. 10 C). V_r was less positive for the EEED mutant than for α_{1G} under all experimental conditions. Extracellular acidification significantly shifted V_r in the mutant channel (even to a larger extent than in α_{1G}) in 2 mM Ca^{2+} and 150 mM $NMDG^+$, but did not affect it either in 2 mM Ca^{2+} and 150 mM Na^+ nor in 20 mM Ca^{2+} (120 mM $NMDG^+$). Substitution of $NMDG^+$ for Na^+ did not significantly change V_r for α_{1G}, but shifted it significantly to more positive potentials for the EEED mutant at pH_e 9.1 and 6.2.

The effects of extracellular Na^+ on the currents through a_{1G} and the EEED mutant T-type channel, in the presence of 2 mM Ca^{2+}, appeared to be pH_e dependent. To quantify these effects, we have calculated the ratio of current amplitudes in Na^+ and $NMDG^+$ ($I(Na^+)/I(NMDG^+)$) at each repolarization voltage, for pH_e 9.1 and 6.2 (Fig. 11). At pH_e 9.1, inward currents through α_{1G} were 25% smaller in the presence of Na^+ than those in the presence of $NMDG^+$, whereas the outward currents were ∼30% larger. The block of inward currents was, however, weaker at pH_e 6.2, especially at very negative potentials. Substitution of $NMDG^+$ by Na^+ increased inward tail currents through

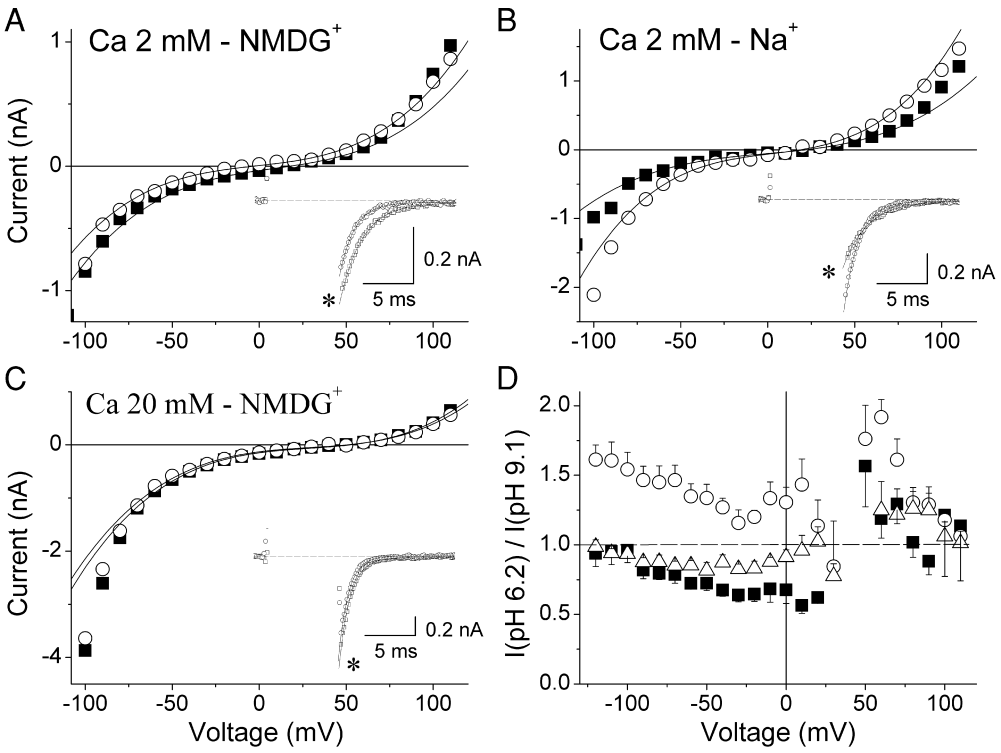

FIGURE 9. Proton effects on the conduction properties of the α_{1G} pore mutant EEED. Voltage dependence of the amplitude of tail currents in a cell expressing the EEED pore mutant at pH_e 9.1 (■) and 6.2 (○) in the presence of: A, 2 mM Ca^{2+} (150 $NMDG^+$); B, 2 mM Ca^{2+} (150 Na^+) and C, 20 mM Ca^{2+} (120 $NMDG^+$). Continuous lines are the best fits with Eq. 2 in the voltage range from −70 to 70 mV. Insets in A–C show current traces at −80 mV in the corresponding perfusion conditions. During the prepulse to 100 mV current values are out of the scale. The asterisks denote the traces obtained at pH_e 9.1. Note the difference in the time scale from that used in Fig. 8. (D) Voltage dependence of the ratio between the amplitude of the tail currents recorded at pH_e 6.2 respect to those in determined at pH_e 9.1 in the presence of 2 mM Ca^{2+} (150 $NMDG^+$) (■), 2 mM Ca^{2+} (150 Na^+) (○) or 20 mM Ca^{2+} (120 $NMDG^+$) (△) (n = 7–10).

the EEED mutant by 25–60% at pH_e 9.1, but this increase was ~150% at pH_e 6.2.

Modulation of Deactivation Kinetics of α_{1G} by Extracellular Protons Is Dependent on Extracellular Ionic Conditions. Effects of Extracellular Ca^{2+} and Na^+

Extracellular acidification consistently accelerated channel deactivation (insets in Fig. 8, A–C, and 9, A–C). We describe here that this effect is also dependent on the $[Ca^{2+}]_e$. Fig. 12, A and B, shows the voltage dependence of the time constant of the current decay (τ_{decay}), estimated from single-exponential fits of tail currents, for α_{1G} and the EEED mutant in 2 mM (150 mM Na^+ or $NMDG^+$) and in 20 extracellular mM Ca^{2+} (120 mM $NMDG^+$). The fit of these data with Eq. 6 yield the parameters that describe the voltage dependence of the time constant of deactivation (τ_{deac}), i.e., the voltage at which τ_{deac} was equal to 1 ms ($V\tau_{deac}$, to describe the position along the voltage axis) and the steepness of the voltage dependence ($s\tau_{deac}$). Fig. 12 C shows that $V\tau'''_{deac}$ was more negative for both channels and pH_e values in the presence of 150 mM Na^+ (2 mM Ca^{2+}), whereas extracellular acidification and 20 mM Ca^{2+} shifted the voltage dependence of τ_{deac} to less negative potentials. At pH_e 6.2 the voltage dependencies in 2 mM and 20 mM Ca^{2+} nearly overlap, suggesting that protons and Ca^{2+} compete to screen and/or bind to the same surface charges as shown for the activation process. As reported for α_{1H} (Delisle and Satin, 2000), extracellular acidification did not significantly modify the voltage sensitivity of the deactivation process ($s\tau_{deac}$) of α_{1G} nor that of the EEED mutant (Fig. 12 D). Interestingly, the EEED mutant showed less negative $V\tau_{deac}$ values and larger $s\tau_{deac}$ than the wild-type channel in all experimental conditions and smaller values of $s\tau_{deac}$ in the presence of 20 mM Ca^{2+} than in 2 mM.

DISCUSSION

Both gating and permeation mechanisms of voltage-dependent Ca^{2+} channels are modulated by ionic conditions and particularly by extracellular protons and Ca^{2+} (Prod'hom et al., 1989; Tytgat et al., 1990; Shuba et al., 1991; Kwan and Kass, 1993; Chen et al., 1996; Polo-Parada and Korn, 1997; Alvarez et al., 2000; Delisle and Satin, 2000; Shah et al., 2001). For T-type Ca^{2+} channels in particular it has been shown previously that extracellular protons shift the voltage dependence of channel activation due to neutralization of surface

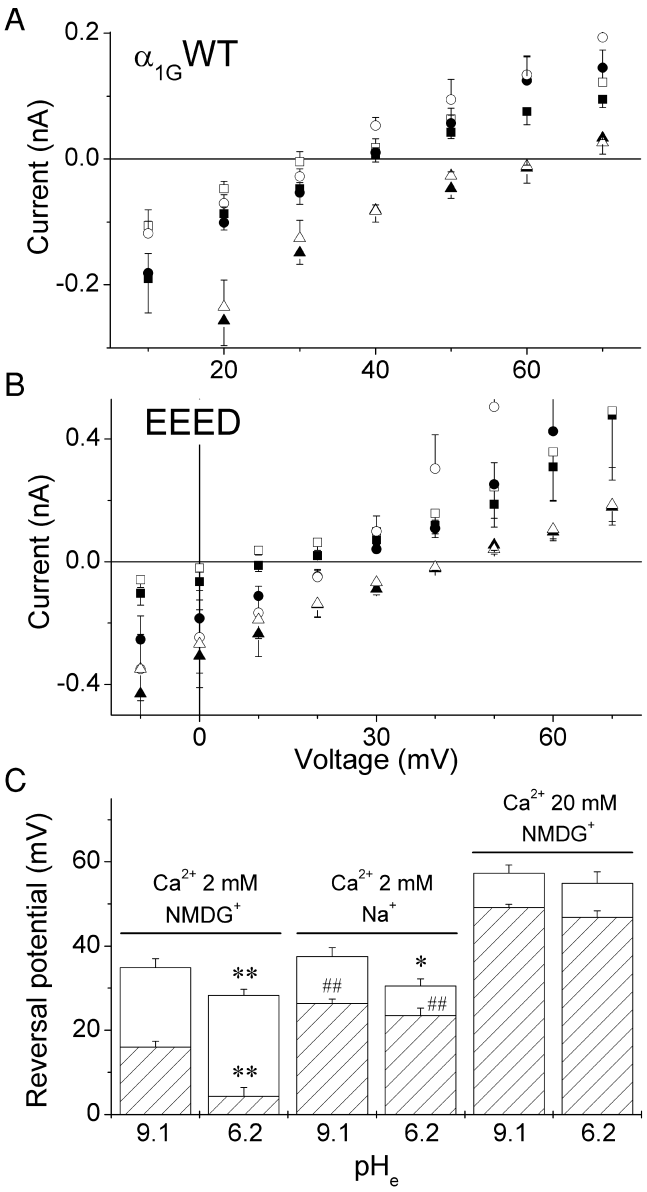

FIGURE 10. Proton effect on reversal potential of α_{1G} and the EEED pore mutant depend on extracellular $[Ca^{2+}]$. (A and B) Voltage dependence of average amplitudes of tail currents though the α_{1G} wild-type and the EEED mutant channels, respectively, at pH_e 9.1 (filled symbols) and 6.2 (open symbols), in the presence of 2 mM Ca^{2+} (150 $NMDG^+$) (■, □), 2 mM Ca^{2+} (150 Na^+) (●, ○) or 20 mM Ca^{2+} (120 $NMDG^+$) (▲, △). (C) Average reversal potentials (V_r) obtained form the fits of the voltage dependence of the amplitude of tail currents through α_{1G} (empty bars) (n = 6–7) and the EEED mutant (dashed bars) (n = 7–10). The different extracellular perfusion conditions are indicated by the horizontal bars. For each channel, the symbols (*) and (**) indicate significant difference between the values at 9.1 and 6.2 with $P < 0.05$ and $P < 0.01$, respectively. Significant difference between the values in Na^+ and $NMDG^+$ with $P < 0.01$ is denoted by (##).

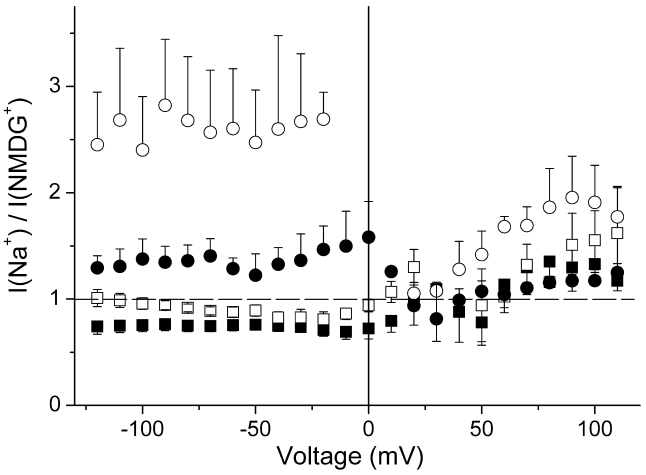

FIGURE 11. Proton-dependent contribution of Na^+ to the permeation through α_{1G} and the EEED pore mutant. Voltage dependence of the ratio between the amplitude of the tail currents recorded in 2 mM Ca^{2+} in the presence of 150 mM extracellular $NMDG^+$ and those obtained in equimolar Na^+ at pH_e 9.1 (filled symbols) or at pH_e 6.2 (empty symbols) (α_{1G}: ■, □, N = 5; EEED: ●, ○, N = 4).

charges and decrease the voltage sensitivity of channel activation, which is not consistent with the surface charge hypothesis (Tytgat et al., 1990; Delisle and Satin, 2000; Shah et al., 2001). In addition, protons either reduce single channel conductance in 110 mM Ca^{2+} (Tytgat et al., 1990), or increase the whole-cell conductance and shift of channel selectivity toward monovalent ions in nearly physiological conditions (2.5 mM Ca^{2+} and 140 mM Na^+) (Delisle and Satin, 2000). Taking into account that Ca^{2+} and protons interact in the modulation of channel gating and ion permeation in HVA Ca^{2+} channels (Kwan and Kass, 1993; Chen et al., 1996; Chen and Tsien, 1997), we were interested to investigate if Ca^{2+} modulates the effects of pH_e on T-type channel function.

Ca^{2+} Inhibits the Effects of Protons on Channel Gating

Tytgat et al. (1990) reported that changes in pH_e from 9 to 6 did not shift the voltage for half-maximal activation V_{act} in the presence of 110 mM Ca^{2+}, but significantly changed it in 5.4 mM Ca^{2+}. In the present study, we show that extracellular acidification induced a shift of V_{act} and increased the slope factor of activation s_{act} in the presence of either 0, 2 or 20 mM Ca^{2+}, and that the magnitudes of these effects were more prominent at lower $[Ca^{2+}]_e$. Remarkably, protons shifted V_{act} to more positive values in Ca^{2+} free solutions than in 2 or 20 mM Ca^{2+} (Fig. 4), indicating that protons induce an extra positive shift in the voltage dependence of the activation process that cannot be explained by the neutralization of surface charges. The shift of V_{act} and increase of s_{act} could be interpreted as a voltage-dependent open pore block by protons (Woodhull, 1973). However, the finding that Ca^{2+}-dependent proton ef-

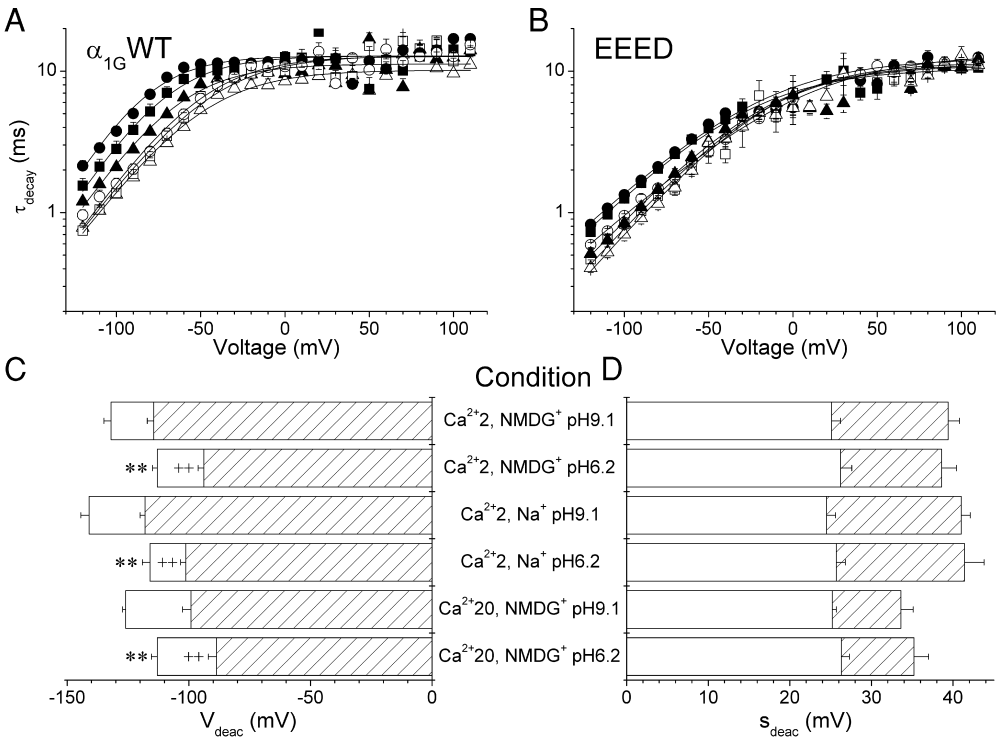

FIGURE 12. Proton modulation of deactivation kinetics of α_{1G} and the EEED pore mutant is dependent on extracellular Ca^{2+}. (A and B) Voltage dependence of the average time constant of the decay (τ_{decay}) of tail currents through α_{1G} (N = 6–7) and the EEED mutant (N = 7–10), respectively, at pH_e 9.1 (filled symbols) and 6.2 (open symbols), in the presence of 2 mM Ca^{2+} (150 $NMDG^+$) (■, □), 2 mM Ca^{2+} (150 Na^+) (●, ○) or 20 mM Ca^{2+} (120 $NMDG^+$) (▲, △). Continuous lines are functions of the form of Eq. 6 calculated using average values of $V\tau_{deac}$, $s\tau_{deac}$ shown in C and D, respectively, and k_{OIo}. The symbols (**) and (++) indicate significant difference between the values at 9.1 and 6.2 with $P < 0.01$ for α_{1G} (empty bars) and the EEED mutant (dashed bars), respectively.

fects on the voltage dependence of τ_{act} were similar to those on steady-state activation indicate that the proton effects on the shape of the current-voltage relationship are to a large extent due to modifications in channel gating. Moreover, the open pore block by protons was proven to be voltage independent when $NMDG^+$ was present in the bath solution. In a more physiological condition (150 mM extracellular Na^+), the voltage dependence of the proton block shows an opposite slope to that expected from a Woodhull-like open pore block (see below).

Extracellular protons also affected inactivation of T-type channels by shifting the voltage for half-maximal inactivation V_{inac}, as it has been reported previously for cardiac T-type Ca^{2+} channels (Tytgat et al., 1990) and the T-type α_{1H} subunit (Delisle and Satin, 2000). Changes in the slope factor of the inactivation curve s_{inac} had not been reported so far. Our results show that extracellular Ca^{2+} antagonizes the effects of pH_e on both V_{inac} and s_{inac} of α_{1G}, in the sense that significant changes in these parameters require larger changes in pH_e at higher Ca^{2+} concentrations. These effects of protons on channel inactivation might be indirect, due to a coupling between activation and inactivation, as discussed in the next section.

Extracellular protons shift the voltage dependence of the time constant of deactivation τ_{deac} of α_{1G} along the voltage axis, in agreement with the results of Delisle and Satin (2000) for α_{1H}. Furthermore, we show that this shift, as for the other gating processes, depends on $[Ca^{2+}]_e$. Delisle and Satin (2000) found similar depolarizing shifts of the activation and deactivation processes for a pH_e change from 8.2 to 5.5 in 2.5 mM Ca^{2+}, and suggested that these might be due to the neutralization of surface charges by extracellular protons. However, a closer examination of the Ca^{2+} effects reveals peculiar features of the proton modulation. With a milder acidification we observed that the proton-induced shift in $V\tau_{deac}$ was larger than that in V_{act} at high $[Ca^{2+}]_e$. Extracellular acidification from pH 9.1 to 6.2 shifted $V\tau_{deac}$ and V_{act}, respectively, by 19 and 20.1 mV in 2 mM Ca^{2+}, but by 13 and 7 mV in 20 mM Ca^{2+} (compare Figs. 4 B and 5 C with Fig. 12 C). We believe that these results are not in contradiction with those of Delisle and Satin (2000) because they worked in proton-favoring conditions that possibly override Ca^{2+} effects. However, our findings cannot be explained by the standard surface potential theory (Frankenhaeuser and Hodgkin, 1957), which implies that protons shift the voltage dependence of all gating parameters by the same amount at each $[Ca^{2+}]_e$. To explain the different proton-induced shifts in voltage dependence of activation and deactivation by the neutralization of surface charges it has to be assumed that this effect is state dependent, in the way that due to structural rearrangements during gating, the channel structure present different substrates for protons and/or different sensitivity of the voltage sensors (or gating machinery) to proton effects (Hille, 2001).

The standard surface-potential theory also predicts that the effects of increasing extracellular proton and Ca^{2+} concentrations on the positive shift of the gating parameters are additive (Kwan and Kass, 1993). Our observation that protons shift the activation curve to more positive potentials in the absence of extracellular Ca^{2+} (Fig. 4, A and B) is therefore incompatible with neutralization of surface charges being the sole mechanism responsible for the shift of activation kinetics. Delisle and Satin (2000) proposed that the reduced voltage sensitivity of activation is due to a proton-induced slowing of voltage dependent transitions distally to channel opening. We have extended this idea to explain our results. First, we propose that protons not only decrease the voltage sensitivity of the activation (increase s_{act}) but also shift the voltage of half-maximal activation to more positive potentials independently of the neutralization of surface charges. Second, we postulate that Ca^{2+} inhibits these effects of protons on activation. On the other hand, in accord with Delisle and Satin (2000), we consider that the transition determining macroscopic deactivation is only modulated by the neutralization of negative surface charges.

We have reported previously that aspartate-to-glutamate mutations in the EEED pore locus of α_{1G} induces changes in the activation curve of the channel (Talavera et al., 2001). The present result demonstrate that the EEED mutant shows alterations in the deactivation process, with less negative $V\tau_{deac}$ values and smaller voltage sensitivity for τ_{deac} than the wild-type channel. These and other gating modifications induced by pore mutations are discussed in the accompanying paper (Talavera et al., 2003, in this issue).

Activation-inactivation Coupling and Proton Effects on Channel Gating

The voltage dependence of the inactivation of T-type Ca^{2+} channels arises from voltage-dependent transitions occurring during channel activation (Droogmans and Nilius, 1989; Chen and Hess, 1990; Serrano et al., 1999; Burgess et al., 2002). Since protons modify the activation process it is interesting to study the possible correlation between the proton-induced changes in the parameters describing steady-state activation and inactivation. We have found that if pH_e is changed in the range of 9.1 to 6.2, for each 1 mV shift in V_{act} there was a 0.4–0.5 mV shift in V_{inac} in both 2 and 20 mM Ca^{2+}. A similar correlation factor was calculated from the data of Delisle and Satin (2000) for α_{1H} (their Figs. 1 D and 2 C). On the other hand, there was no strict correlation between the voltage sensitivity of inactivation (s_{inac}) and activation (s_{act}) and between s_{inac} and V_{inac}, in contrast with that observed between s_{act} and V_{act} (see Fig. 7). Thus, although proton-induced changes in the inactivation and activation processes seem to be linked, their degree of correlation is not absolute. As we discuss below, a kinetic model that includes state-dependent proton effects can explain these results.

A Kinetic Model Predicts State-dependent Effects of Extracellular Protons and Ca^{2+}

Currently, there are several kinetic models of T-type channel gating (Droogmans and Nilius, 1989; Chen and Hess, 1990; Serrano et al., 1999; Burgess et al., 2002). The model of Burgess et al. (see Fig. 13) is particularly attractive since it accounts for the properties of the α_{1G} and α_{1H} channels in nearly physiological conditions and includes for the first time an explicit description of the gating charges associated with channel transitions. We adopted this model and determined which parameters had to be modified in order to describe our experimental data in the different pH_e in the presence of 2 or 20 mM Ca^{2+}. First, we readjusted the parameters of the original model to describe our own experimental data at pH_e 7.4 in 2 mM Ca^{2+} (see Table I). We then considered as working hypothesis that the modifications of gating induced by H^+ and Ca^{2+} are due to: (a) the neutralization of surface charges, (b) state-dependent alterations of the electric field sensed by the gating charges, and (c) the modification of the gating charges. To evaluate these effects independently from each other we used the following approach. All voltage-dependent transitions, with the exception of the deactivation transitions ($O \rightarrow C_3$ and $I_O \rightarrow I_3$), were rewritten as:

$$k_{C1C2} = K_{C1C2}\exp\left[\frac{\delta_1 q_1}{T}(V - V_{Shift})\right];$$

$$k_{C2C1} = K_{C2C1}\exp\left[-\frac{(1-\delta_1) q_1}{T}(V - V_{Shift})\right]$$

$$k_{I1I2} = K_{I1I2}\exp\left[\frac{\delta_1 q_1}{T}(V - V_{Shift})\right];$$

$$k_{I2I1} = K_{I2I1}\exp\left[-\frac{(1-\delta_1) q_1}{T}(V - V_{Shift})\right]$$

$$k_{C2C3} = K_{C2C3}\exp\left[\frac{\delta_2 q_2}{T}(V - V_{Shift} - V_{O2})\right];$$

$$k_{C3C2} = K_{C3C2}\exp\left[-\frac{(1-\delta_2) q_2}{T}(V - V_{Shift} - V_{O2})\right]$$

$$k_{I2I3} = K_{I2I3}\exp\left[\frac{\delta_2 q_2}{T}(V - V_{Shift} - V_{O2})\right];$$

$$k_{I3I2} = K_{I3I2}\exp\left[-\frac{(1-\delta_2) q_2}{T}(V - V_{Shift} - V_{O2})\right],$$

where $T = 25.4$ mV is the thermal energy in electron-volts, q_1 and q_2 are the gating charges associated with the first and second boxes of the kinetic scheme, and δ_1 and δ_2 account for the coupling between the local electric potential sensed by q_1 and q_2 and the membrane

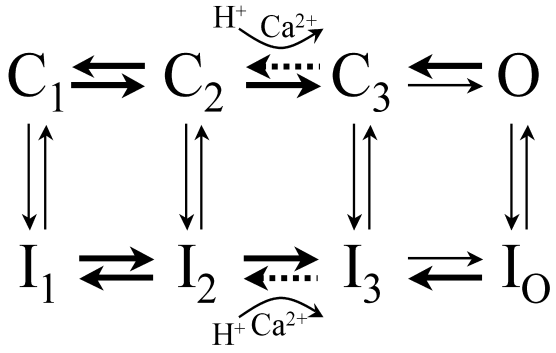

FIGURE 13. Kinetic scheme of the Markov model used to describe the proton and Ca^{2+} modulation of the gating of α_{1G}. The states C_1 (resting) and I_1 (inactivated) are the most probable at very negative potentials (less than or equal to −100 mV). Membrane depolarization induces transitions to the intermediate closed states C_2 and C_3 and to the open state O. In parallel, the channel transits to the inactivated states I_2, I_3 and for strong depolarizations the equilibrium shifts to the inactivated state I_O. All voltage dependent transitions (represented by the thick arrows) are affected by the neutralization of negative surface charges by protons or Ca^{2+}. The fit of the model to the data obtained at different pH_e indicate that the transitions $C_3 \rightarrow C_2$ and $I_3 \rightarrow I_2$ (dashed arrows) are the main target for proton effects leading to the decrease of the voltage sensitivity of activation. Extracellular Ca^{2+} is proposed to inhibit the effects of protons on these transitions.

potential *V*. We introduced a voltage offset (V_{Shift}) in all these rate constants to describe the neutralization of surface charges. To account for the state-dependent modification of the electric field sensed by the gating charges, we included the voltage offset V_{O2} in the second box of the kinetic scheme (see Fig. 13). Starting from the set of parameters obtained at pH_e 7.4 and 2 mM Ca^{2+} (Table I), we adapted the parameters V_{Shift}, V_{O2}, q_1, q_2, and k_{C3O} to fit the average activation, steady-state inactivation, reactivation curves and the voltage dependence of the time-to-peak obtained in each experimental condition. The variation of δ_1 and δ_2 did not significantly affect the goodness of the fits and thus they were kept fixed to the values obtained in the reference condition. We introduced an extra voltage offset in order to account for the neutralization of surface charges by Ca^{2+} to fit the data obtained in 20 mM Ca^{2+}. This value was set to 20.5 mV and taken from the shift of the voltage of half-maximal activation by changing the $[Ca^{2+}]_e$ from 2 to 20 mM at pH_e 9.1 (see Fig. 4 B).

The deactivation transitions $O \rightarrow C_3$ and $I_O \rightarrow I_3$ were described by an equation of the form: $k_{OC3} = k_{IOI3} = \exp[-(V - V\tau_{deac})/s\tau_{deac}]$, where $V\tau_{deac}$ ($= T/q_3 \ln(K_{OC3})$) and $s\tau_{deac}$ ($= T/q_3$) are the experimental values at each pH_e and $[Ca^{2+}]_e$ (e.g., Fig. 12). The parameter V_{Shift} is not included in the expressions of k_{OC3} and k_{IOI3} because the effect of neutralization of surface charges is implicitly considered in the values of $V\tau_{deac}$.

TABLE I

Model Parameters Optimized to Fit the Experimental Data Obtained at pHe 7.4 in the Presence of 2 mM Extracellular Ca^{2+}

Parameter	Value	Parameter	Value
q_1	1.28	δ_1	0.819
q_2	3.73	δ_2	0.128
q_3	0.984	δ_3	0
K_{C1C2}	2.85	K_{C2C1}	1.11
K_{C2C3}	17.9	K_{C3C2}	0.105
$k_{C3O} = k_{I3Io}$	2.80	$K_{OC3} = K_{IoI3}$	7.60×10^{-3}
K_{I1I2}	0.0240	K_{I2I1}	4.35×10^{-3}
K_{I2I3}	0.573	K_{I3I2}	2.50×10^{-5}
k_{C1I1}	9.93×10^{-4}	k_{I1C1}	3.31×10^{-4}
k_{C2I2}	0.0120	k_{I2C2}	1.86×10^{-3}
$k_{OIo} = k_{C3I3}$	0.09	$k_{IoO} = k_{I3C3}$	1.04×10^{-4}

Fig. 14 shows that the simulated curves of steady-state activation and inactivation reproduce the experimental data in the pH_e range of 9.1 to 6.2–5.5 and in the presence of 2 or 20 mM Ca^{2+}. The parameters optimized with the fitting procedure are shown as functions of pH_e and Ca^{2+} in Fig. 15. V_{Shift}, which describes the proton-induced voltage shift due to the neutralization of surface charges, is equal to −5.5 mV at pH_e 9.1 and gradually changes to positive values at acid pH_e in 2 mM Ca^{2+} (panel A). Panel B exemplifies that this causes an identical displacement of all the gating kinetics to less negative potentials. Fig. 15 C shows that V_{O2} is around −4 mV at alkaline pH_e but changes to positive values at acid pH_e in 2 mM Ca^{2+}. This induces an additional positive shift of the inactivation and activation curves and a slight increase in the steepness of the latter one (panel B). The relevance of the introduction of V_{O2} in the model becomes clear when noticing that the voltage shift attributable to the screening of surface charges when changing the pH_e from 9.1 to 6.2 ($V_{Shift}(6.2) - V_{Shift}(9.1) \approx 19$ mV, Fig. 15 A) equals the shift observed in the voltage dependence of the time constant of deactivation (Fig. 12 C). In other words, V_{O2} allows dissecting the effect of pure screening of surface charges from specific proton effects on channel activation. The specificity of this voltage offset on the transitions between the states C_2 and C_3 may be due to an enhanced accessibility or/and an increased affinity of superficial binding sites for protons during these transitions. Another possibility is that protonation induces an uncoupling between the voltage sensors and the activation gates of the channel. The appropriate fit of the data requires the reduction of the gating charge. However, the gating charge associated with the second step of activation (q_2) shows a much stronger pH_e dependence than that associated with the first step (q_1). In 2 mM Ca^{2+} for example, q_2 shows a marked reduction in the whole pH_e range studied, whereas q_1 does not change in the pH_e range from 9.1 to 6.8 (Fig. 15 E).

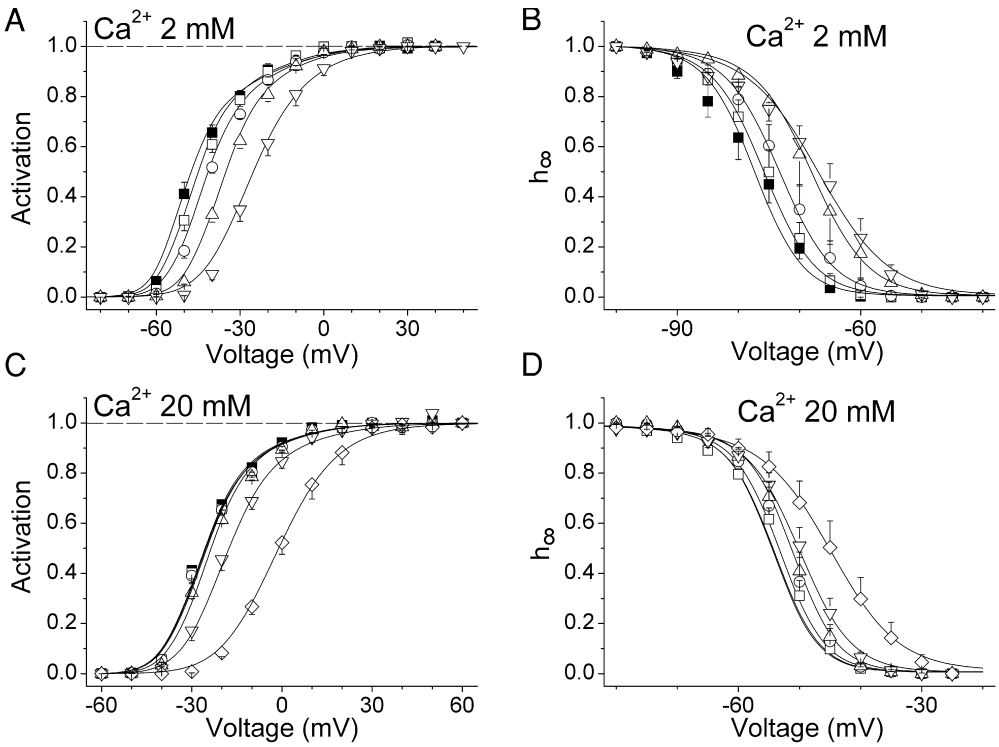

FIGURE 14. Fit of the kinetic model to the experimental data. Fit of average activation (A and C) and inactivation (B and D) curves obtained in the presence of 2 or 20 mM Ca^{2+}. The symbols apply to pH_e values as follows: 9.1, ■; 8.2, □; 7.4, ○; 6.8, △; 6.2, ▽; 5.5, ◇.

As shown in panel D, the predicted decrease in q_1 does not have large effect on the steady-state properties in contrast to the reduction of q_2, which induces a decrease in the slope of activation and inactivation curves (panel F). The decrease in q_2 shifts the inactivation curve to more negative potentials in a larger extent than the activation curve. This is, therefore, based on the application of the present gating model, the reason for the uneven effects of extracellular protons on activation and inactivation properties of α_{1G} (Fig. 7). The fit of the voltage dependence of the time-to-peak compelled a decrease of the rate of the last step of the activation (k_{C3O} and k_{I3O}) in the ranges from 4.6 to 1.9 ms^{-1} in 2 mM Ca^{2+} and from 2.4 to 1.2 ms^{-1} in 20 mM Ca^{2+}. This produces a positive shift of the activation and inactivation curves and an increase of the steepness of the activation curve (compare dotted and short dashed lines in Fig. 15 F).

The results of the simulation of the data obtained in 20 mM Ca^{2+} indicate that predicted effects of protons in this condition are much weaker than in 2 mM Ca^{2+}. We conclude that calcium ions antagonize the effects of extracellular protons on the gating properties of α_{1G} in two ways: first, by competing for the binding to negative surface charges and, second, by controlling the proton-induced effects on an intermediate step of the activation sequence. In the first mechanism Ca^{2+} and protons have equivalent effects, since both ions neutralize negative surface charges and shift all voltage-dependent processes of the channel toward positive potentials. The inhibition of channel activation by the binding of protons through the second mechanism is weakened by the presence of Ca^{2+}, which could be due to a decreased proton affinity or a modulation of the effects downstream of proton binding. This may explain why the increase of $[Ca^{2+}]_e$ prevents the decreased voltage sensitivity, the "extra" voltage shift of the activation induced by protons that is observed in Ca^{2+} free conditions (Fig. 4) and the smaller proton-induced shift of the activation curves with respect to that of the voltage dependence of the deactivation kinetics. The next section argues for the selectivity filter as a target for protonation, but, as demonstrated in the accompanying paper, the binding of protons to the EEDD pore locus is not related to the proton-induced modification of channel activation.

Proton Effects on Permeation and Selectivity of α_{1G} Are Dependent on Ca^{2+}, Na^+, and the Structure of the Selectivity Filter

Tytgat et al. (1990) reported that extracellular acidification reduces the conductance of single cardiac T-type channels in the guinea pig. However, Delisle and Satin (2000) concluded that protons do not block the α_{1H} channel, but actually increase the whole-cell conductance and decrease the Ca^{2+}/monovalent cation selectivity. These discrepant results might be reconciled by the different extracellular Ca^{2+} and Na^+ concentrations that were used in these reports. In fact, it has been shown that ion conduction through Ca^{2+} channels depends on both Ca^{2+} and Na^+ concentrations

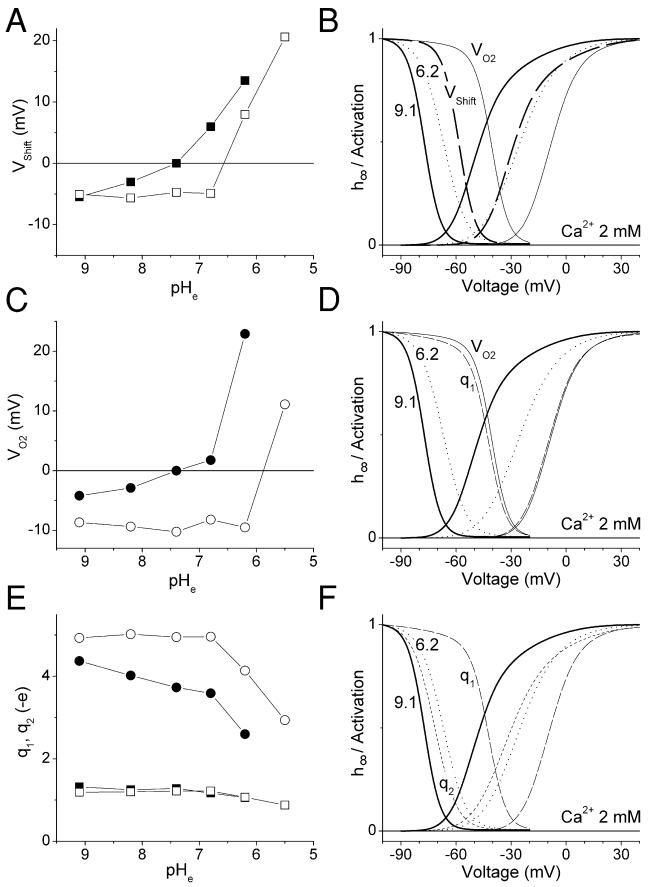

FIGURE 15. pH$_e$ and Ca^{2+} dependence of the model parameters optimized to fit the experimental data. (A) Predicted pH$_e$ dependency of V_{Shift} in the presence of 2 (■) or 20 mM (□) Ca^{2+}. (B) Activation and inactivation curves calculated with the parameters from the fit of the data obtained in 2 mM Ca^{2+} at pH$_e$ 9.1 (thick continuous lines) or 6.2 (dotted lines). The thick dashed and the thin continuous lines are the activation and inactivation curves calculated with the set of parameters determined for pH$_e$ 9.1 (Ca^{2+} 2 mM) but with the values of V_{Shift} or with both V_{Shift} and V_{O2} obtained for pH$_e$ 6.2, respectively. (C) V_{O2} as function of pH$_e$ in the presence of 2 (●) or 20 mM (○) Ca^{2+}. (D) The thick continuous, thin continuous, and dotted lines are the same as in B. The thin dashed lines were calculated using the set of parameters at pH$_e$ 9.1 (Ca^{2+} 2 mM), but using the values of V_{Shift}, V_{O2}, and q_1 determined for pH$_e$ 6.2. (E) Predicted pH$_e$ dependency of q_1 (■, □) and q_2 (●, ○) in the presence of 2 (filled symbols) or 20 mM (empty symbols) Ca^{2+}. (F) The thick continuous, thin dashed and dotted lines are the same as in D. The short dashed lines were calculated using the set of parameters at pH$_e$ 9.1 (Ca^{2+} 2 mM) but using the values of V_{Shift}, V_{O2}, q_1, and q_2 determined for pH$_e$ 6.2.

(Polo-Parada and Korn, 1997) and that Na$^+$ can contribute significantly to the current through T-type channels (Lee et al., 1999; Serrano et al., 1999). Our data about the effects of extracellular Ca^{2+} and Na$^+$ on the open pore block and the changes in ion selectivity induced by protons in α_{1G} and the EEED pore mutant support this contention.

We have found that in α_{1G}, extracellular acidification from pH 9.1 to 6.2 decreased the amplitude of inward tail currents by ~33% in the presence of 2 mM Ca^{2+} (150 NMDG$^+$), whereas the block was maximal 10% in 20 mM Ca^{2+}, indicating that open-pore proton block is larger at low [Ca^{2+}]$_e$. Analogue experiments with the EEED pore mutant confirmed that open-pore proton block is Ca^{2+} dependent and showed that proton block of Ca^{2+} conduction (20 mM Ca^{2+}) was stronger than in the wild-type channel.

The reversal potentials were less positive in the EEED mutant than in the wild-type channel under all conditions, in agreement with our previous findings (Talavera et al., 2001). The fact that this was observed at pH$_e$ 9.1 may indicate that the EEED mutant has a decreased Ca^{2+} selectivity respect to α_{1G}, independently from the channel protonation. This hypothesis would mean that the exchange of the aspartate residue D1487 for glutamate disrupts the coordination of Ca^{2+} binding to the selectivity filter in contrast to the results in L-type Ca^{2+} channels (Ellinor et al., 1995). A second possibility is that some protonation occurs at nanomolar extracellular proton concentrations, implying a much higher proton affinity of the EEED arrangement in the α_{1G} template than in that of the L-type channel (Chen and Tsien, 1997). This hypothesis fits nicely with previous evidence suggesting that an EEEE selectivity filter in the α_{1G} channel impose a narrower ionic pathway than in HVA channels (Talavera et al., 2001), which is in turn in agreement with the fact that the pore of the wild-type T-type channels is narrower than that of HVA Ca^{2+} channels (Cataldi et al., 2002). In both α_{1G} and the EEED mutant, the proton-induced decrease of the Ca^{2+}/monovalent cation selectivity (judged by the negative shift of the reversal potential) was observed in 2 but not in 20 mM Ca^{2+}. For the EEED mutant, the negative shift of the reversal potential in 2 mM Ca^{2+} was not observed in the presence of Na$^+$, probably because in this condition the channel selectivity for monovalent cations is so high that extracellular acidification does not further increase it, in contrast with the observations in the wild-type channel (Fig. 10 C).

Intriguingly, Delisle and Satin (2000) found that extracellular acidification increased the macroscopic conductance of the T-type channel α_{1H}. Suspecting that this was due to the presence of extracellular Na$^+$, we also addressed the effects of sodium ions on proton block and permeation through α_{1G}. We found that the proton block in the presence of 150 mM Na$^+$ and 2 mM Ca^{2+} was significantly reduced at negative potentials compared with that in 150 mM NMDG$^+$, suggesting that channel protonation increased the Na$^+$ permeation through the channel (Fig. 8). Interestingly, the substitution of NMDG$^+$ by Na$^+$ did not significantly change the reversal potential of α_{1G}, in contrast with the significant shift to positive potentials of V_r in the EEED mutant at pH$_e$ 9.1 and 6.2 (Fig. 10). On the

other hand, the comparison of the amplitude of the tail currents recorded in the presence of $NMDG^+$ or Na^+ (Fig. 11) indicates that under alkaline conditions extracellular Na^+ blocks inward current through a_{1G}, whereas Na^+ appears to contribute to the inward current in acid extracellular medium. These observations are in agreement with the previous finding that variations of extracellular Na^+ do not change the basal T-type current in cardiac cells at pH_e 7.4 (Alvarez et al., 2000). In the EEED mutant, substitution of $NMDG^+$ by Na^+ increased inward currents, in accord with the significant enhancement of Na^+ selectivity deduced from the changes in reversal potentials.

Notably, the proton block of the Ca^{2+} permeation through α_{1G} did not show voltage dependence and the same was the case for the effects of the substitution of $NMDG^+$ by Na^+ for both α_{1G} and the EEED mutant. These results suggest that the site of protonation and Na^+ binding senses very little of the membrane electric field. The voltage dependence of the proton block in the wild-type channel in the presence of extracellular Na^+ and in the EEED mutant are likely to be related to the proton-induced increase of the monovalent conduction at very negative potentials.

The evidence gathered from the L-type Ca^{2+} channel indicate that channel protonation controlling permeation properties occurs at the selectivity filter of this channel, i.e., the carboxilates of the EEEE pore locus (Chen et al., 1996; Klockner et al., 1996; Chen and Tsien, 1997; Varadi et al., 1999), rather than at a site modulating channel conductance via an allosteric mechanism (Prod'hom et al., 1989; Kuo and Hess, 1993). Taken together, we can conclude that in T-type Ca^{2+} channels, (a) the open pore block of the Ca^{2+} conduction and the decrease of the Ca^{2+}/monovalent cations selectivity induced by protons depend on the $[Ca^{2+}]_e$, (b) at low pH_e monovalent cations contribute significantly to the conduction, (c) protonation leading to a modification of conduction occurs at the EEDD pore locus, and (d) the EEDD pore locus is located close to the extracellular face of the channel. We propose that protonation of glutamate and/or aspartate residues neutralizes part of the negative charge of the selectivity filter and reduces the affinity for Ca^{2+}, decreasing Ca^{2+}/monovalent cation selectivity. It is reasonable to think that protonation of the selectivity filter of Ca^{2+} channels might mimic the structure of the selectivity filter of sodium channels, which is built by a far less electronegative DEKA locus.

Functional Significance of Proton–Ca^{2+} Interaction

We propose that protons and Ca^{2+} modulate T-type channel gating by two mechanisms. First, both ions shift the voltage-dependent kinetics by neutralizing negative surface charges; and second, Ca^{2+} prevents the proton-induced inhibition of channel activation. The potential patho-physiological implications of the proton modulation of T-type channels has been associated with the activity of the thalamocortical network (Shah et al., 2001), the pacemaker function (Tytgat et al., 1990), and the generation of arrhythmias (Delisle and Satin, 2000) in cardiac tissue. In this context the consequences of the interrelated modifications of the activation and the inactivation of T-type channels by extracellular protons are particularly interesting. Ischemic and hypoxic conditions induce both extracellular acidification and cell depolarization in cardiac and nervous tissues. Thus, the coupled shift of steady-state activation and inactivation in extracellular acidification results in a concomitant shift of the T-type window current along the voltage axis in the direction of the change of the basal membrane potential. This means that, although protons reduce channel activation, the Ca^{2+} entry through T-type channels could be preserved during extracellular acidification, which in turn might regulate cellular functions by constant injection of inward current and the increase in intracellular Ca^{2+} concentration. On the other hand, we can speculate that the uneven proton effects on activation and inactivation properties, as well as the proton-induced change in channel selectivity toward monovalent ions and the block of Ca^{2+} permeation could protect against harmful Ca^{2+} overload.

We thank Dr. F. Hofmann for the α_{1G} clone and Dr. M. Staes for the help in the construction of the α_{1G} pore mutant. We are also grateful to Drs. J.L. Alvarez, G. Vassort, T. Voets, and R. Vennekens for helpful discussions. The expert technical assistance of M. Crabbé, H. Van Weijenbergh, S. de Swaef, and M. Schuermans is greatly acknowledged. We also thank Professor V. Flockerzi for providing the vector pCAGGSM2.

This work was supported by the Belgian Federal Government, the Flemish Government, and the Onderzoeksraad KU Leuven (GOA 99/07, F.W.O. G.0237.95, F.W.O. G.0214.99, F.W.O. G. 0136.00; Interuniversity Poles of Attraction Program, Prime Ministers Office IUAP).

Olaf S. Andersen served as editor.

Submitted: 9 January 2003
Revised: 21 April 2003
Accepted: 25 April 2003

REFERENCES

Alvarez, J.L., A. Artiles, K. Talavera, and G. Vassort. 2000. Modulation of voltage-dependent facilitation of the T-type calcium current by sodium ion in isolated frog atrial cells. *Pflugers Arch.* 441: 39–48.

Burgess, D.E., O. Crawford, B.P. Delisle, and J. Satin. 2002. Mechanism of inactivation gating of human T-type (low-voltage activated) calcium channels. *Biophys. J.* 82:1894–1906.

Carbone, E., and H.D. Lux. 1987. Single low-voltage-activated calcium channels in chick and rat sensory neurones. *J. Physiol.* 386: 571–601.

Cataldi, M., E. Perez-Reyes, and R.W. Tsien. 2002. Differences in apparent pore sizes of low and high voltage-activated Ca2+ channels. *J. Biol. Chem.* 277:45969–45976.

Chen, C.F., and P. Hess. 1990. Mechanism of gating of T-type calcium channels. *J. Gen. Physiol.* 96:603–630.

Chen, X.H., I. Bezprozvanny, and R.W. Tsien. 1996. Molecular basis of proton block of L-type Ca^{2+} channels. *J. Gen. Physiol.* 108:363–374.

Chen, X.H., and R.W. Tsien. 1997. Aspartate substitutions establish the concerted action of P-region glutamates in repeats I and III in forming the protonation site of L-type Ca^{2+} channels. *J. Biol. Chem.* 272:30002–30008.

Delisle, B.P., and J. Satin. 2000. pH modification of human T-type calcium channel gating. *Biophys. J.* 78:1895–1905.

Droogmans, G., and B. Nilius. 1989. Kinetic properties of the cardiac T-type calcium channel in the guinea- pig. *J. Physiol.* 419: 627–650.

Ellinor, P.T., J. Yang, W.A. Sather, J.F. Zhang, and R.W. Tsien. 1995. Ca^{2+} channel selectivity at a single locus for high-affinity Ca^{2+} interactions. *Neuron.* 15:1121–1132.

Frankenhaeuser, B., and A.L. Hodgkin. 1957. The action of calcium on the electrical properties of squid axons. *J. Physiol.* 137: 218–244.

Hille, B. 2001. Ion Channels of Excitable Membranes. 3rd edition. Sinauer Associates, Inc., Sunderland, MA. 646–662.

Klockner, U., G. Mikala, A. Schwartz, and G. Varadi. 1996. Molecular studies of the asymmetric pore structure of the human cardiac voltage-dependent Ca^{2+} channel. Conserved residue, Glu-1086, regulates proton-dependent ion permeation. *J. Biol. Chem.* 271:22293–22296.

Klugbauer, N., E. Marais, L. Lacinova, and F. Hofmann. 1999. A T-type calcium channel from mouse brain. *Pflugers Arch.* 437: 710–715.

Kuo, C.C., and P. Hess. 1993. Characterization of the high-affinity Ca^{2+} binding sites in the L-type Ca^{2+} channel pore in rat phaeochromocytoma cells. *J. Physiol.* 466:657–682.

Kwan, Y.W., and R.S. Kass. 1993. Interactions between H^+ and Ca^{2+} near cardiac L-type calcium channels: evidence for independent channel-associated binding sites. *Biophys. J.* 65:1188–1195.

Lacinova, L., N. Klugbauer, and F. Hofmann. 2002. Gating of the expressed Cav3.1 calcium channel. *FEBS Lett.* 531:235–240.

Lee, J.H., J.C. Gomora, L.L. Cribbs, and E. Perez-Reyes. 1999. Nickel block of three cloned T-type calcium channels: low concentrations selectively block alpha1H. *Biophys. J.* 77:3034–3042.

Nilius, B. 1992. T-type calcium channels in cardiac muscle: News in kinetics and modulation. *In* Intracellular Regulation of Ion Channels. Vol. H 60. Z. Morad, editor. Springer-Verlag, Berlin. 181–189.

Pietrobon, D., B. Prod'hom, and P. Hess. 1989. Interactions of protons with single open L-type calcium channels. pH dependence of proton-induced current fluctuations with Cs^+, K^+, and Na^+ as permeant ions. *J. Gen. Physiol.* 94:1–21.

Polo-Parada, L., and S.J. Korn. 1997. Block of N-type calcium channels in chick sensory neurons by external sodium. *J. Gen. Physiol.* 109:693–702.

Prod'hom, B., D. Pietrobon, and P. Hess. 1989. Interactions of protons with single open L-type calcium channels. Location of protonation site and dependence of proton-induced current fluctuations on concentration and species of permeant ion. *J. Gen. Physiol.* 94:23–42.

Serrano, J.R., S.R. Dashti, E. Perez-Reyes, and S.W. Jones. 2000. Mg^{2+} block unmasks Ca^{2+}/Ba^{2+} selectivity of alpha1G T-type calcium channels. *Biophys. J.* 79:3052–3062.

Serrano, J.R., E. Perez-Reyes, and S.W. Jones. 1999. State-dependent inactivation of the alpha1G T-type calcium channel. *J. Gen. Physiol.* 114:185–201.

Shah, M.J., S. Meis, T. Munsch, and H.C. Pape. 2001. Modulation by extracellular pH of low- and high-voltage-activated calcium currents of rat thalamic relay neurons. *J. Neurophysiol.* 85:1051–1058.

Shuba, Y.M., V.I. Teslenko, A.N. Savchenko, and N.H. Pogorelaya. 1991. The effect of permeant ions on single calcium channel activation in mouse neuroblastoma cells: ion-channel interaction. *J. Physiol.* 443:25–44.

Smirnov, S.V., G.A. Knock, A.E. Belevych, and P.I. Aaronson. 2000. Mechanism of effect of extracellular pH on L-type Ca^{2+} channel currents in human mesenteric arterial cells. *Am. J. Physiol. Heart Circ. Physiol.* 279:H76–H85.

Staes, M., K. Talavera, N. Klugbauer, J. Prenen, L. Lacinova, G. Droogmans, F. Hofmann, and B. Nilius. 2001. The amino side of the C-terminus determines fast inactivation of the T- type calcium channel alpha1G. *J. Physiol.* 530:35–45.

Talavera, K., J. Alvarez, and G. Vassort. 1998. A model of Ca ion permeation through the cardiac T-type Ca-channel. *Biophys. J.* 74: A108.

Talavera, K., M. Staes, A. Janssens, N. Klugbauer, G. Droogmans, F. Hofmann, and B. Nilius. 2001. Aspartate residues of the Glu-Glu-Asp-Asp (EEDD) pore locus control selectivity and permeation of the T-type Ca^{2+} channel alpha(1G). *J. Biol. Chem.* 276:45628–45635.

Talavera, K., A. Janssens, N. Klugbauer. G. Droogmans, and B. Nilius. 2003. Pore structure influences gating properties of the T-type Ca^{2+} channel α_{1G}. *J. Gen Physiol.* 121:529–540.

Tombaugh, G.C., and G.G. Somjen. 1996. Effects of extracellular pH on voltage-gated Na^+, K^+ and Ca^{2+} currents in isolated rat CA1 neurons. *J. Physiol.* 493:719–732.

Tytgat, J., B. Nilius, and E. Carmeliet. 1990. Modulation of the T-type cardiac Ca channel by changes in proton concentration. *J. Gen. Physiol.* 96:973–990.

Varadi, G., M. Strobeck, S. Koch, L. Caglioti, C. Zucchi, and G. Palyi. 1999. Molecular elements of ion permeation and selectivity within calcium channels. *Crit. Rev. Biochem. Mol. Biol.* 34:181–214.

Woodhull, A.M. 1973. Ionic blockage of sodium channels in nerve. *J. Gen. Physiol.* 61:687–708.

Zhou, W., and S.W. Jones. 1996. The effects of external pH on calcium channel currents in bullfrog sympathetic neurons. *Biophys. J.* 70:1326–1334.